

**IMPROVING MECHANICAL PROPERTIES OF  
ADHESIVE JOINTS IN CARBON FIBER  
REINFORCED POLYMER COMPOSITES BY  
INCORPORATION OF GRAPHENE ADDED  
ELECTROSPUN POLYMERIC NANOFIBERS**

**A Thesis Submitted to  
the Graduate School of  
İzmir Institute of Technology  
in Partial Fulfilment of the Requirements for the Degree of**

**MASTER OF SCIENCE**

**in Mechanical Engineering**

**by  
Melisa YEKE**

**July 2023  
İZMİR**

We approve the thesis of **Melisa YEKE**

**Examining Committee Members:**

---

**Prof. Dr. Metin TANOĐLU**

Department of Mechanical Engineering, İzmir Institute of Technology

---

**Assoc. Prof. Dr. Murat BARIŐIK**

Department of Mechanical Engineering, İzmir Institute of Technology

---

**Assoc. Prof. Dr. Levent AYDIN**

Department of Mechanical Engineering, İzmir Katip Çelebi University

**20 July 2023**

---

**Prof. Dr. Metin TANOĐLU**

Supervisor, Department of Mechanical Engineering,  
İzmir Institute of Technology

---

**Prof. Dr. M. İ. Can DEDE**

Head of the Department of Mechanical  
Engineering

---

**Prof. Dr. Mehtap Eanes**

Dean of the Graduate School

## ACKNOWLEDGMENTS

I would like to thank my esteemed thesis advisor, Prof. Dr. Metin TANOĞLU, who guided me with his knowledge and experience throughout my thesis work. I would also like to thank the valuable thesis juries, Assoc. Prof. Dr. Murat BARIŞIK and Assoc. Prof. Dr. Levent AYDIN for their interest in my thesis defense.

I would like to thank the Scientific and Technological Research Council of Turkey (TÜBİTAK) for its support of my thesis within the scope of the 1003 TÜBİTAK project (project number 218M701). I would also like to thank my TÜBİTAK project committee members, Assoc. Prof. Dr. Engin AKTAŞ and Assoc. Prof. Dr. Murat BARIŞIK for their contributions to my work.

I would like to thank Turkish Aerospace Industries Inc. (TUSAŞ) for its material supply.

I would also like to thank IZTECH Center for Materials Research (MAM) for their contribution to the material analysis of this thesis.

I would like to thank Assoc. Prof. Dr. Sevgi KILIÇ ÖZDEMİR for allowing me to use the sonicator device in their laboratory during my thesis work.

I would like to thank my teammates Muhammed Erdal ULAŞLI, Dora ÖZARSLAN, Kaan NUHOĞLU, Mert ÖZKAN, and Seçkin MARTİN who supported me throughout my thesis work.

I would like to thank Dr. Aref CEVAHİR, who guided me with his knowledge and experience throughout my thesis, supported and encouraged me, and contributed to my work with his constructive comments.

I would like to thank İsmail Gürkan DEMİRKIRAN and Rana Başak SERİM who motivated and supported me throughout my thesis work.

Foremost, I would like to thank my mother Gülser ENGİNDENİZ, my aunt Kevser ENGİNDENİZ, my cousin Ömer ENGİNDENİZ and my uncle Veysel ENGİNDENİZ who have loved, supported and encouraged me throughout my life and have always supported my education life.

## ABSTRACT

### IMPROVING MECHANICAL PROPERTIES OF ADHESIVE JOINTS IN CARBON FIBER REINFORCED POLYMER COMPOSITES BY INCORPORATION OF GRAPHENE ADDED ELECTROSPUN POLYMERIC NANOFIBERS

Since composites joined with mechanical fasteners cause severe delamination damage, stress concentration in the joint area, and weight increase, joining composite materials with innovative methods have recently gained more importance. These joining methods prevent delamination damage, provide a uniform distribution of stress, and do not cause considerable weight increases. However, modifying the surface of composite parts joined by innovative methods is critical.

In this study, the bonding surface was modified by coating carbon/epoxy prepregs with electrospun nanofibers with 10% wt/v ratio of PA 66 and 1%, 2% and 3% wt/v ratio of rGO added. Composite parts were joined in the hot press by the secondary bonding method using 3 plies of FM 300K film adhesive. The morphological structure of nanofibers and the dispersion of rGO were analyzed by SEM. The thermal properties of nanofibers were analyzed by DSC. The contact angle measurement device was used to determine the hydrophilic and hydrophobic properties of the unmodified prepreg and nanofiber-modified prepreg surface. The most hydrophilic surface was observed on the nanofiber-coated surface with 2% rGO added. Single Lap Joints (SLJ), and Charpy Impact tests were performed to examine the mechanical properties of modified and unmodified composite plates. According to the SLJ and Charpy Impact results, an improvement of 17.89% and 30.59% was observed in carbon/epoxy composite plates whose surface was modified with 2% rGO, respectively.

# ÖZET

## KARBON FİBER TAKVİYELİ POLİMER KOMPOZİTLERDE YAPIŞTIRICI BAĞLANTILARIN MEKANİK ÖZELLİKLERİNİN GRAFEN İLAVELİ ELEKTRO-EĞRİLMİŞ POLİMERİK NANOLİFLERİN EKLENMESİ İLE İYİLEŞTİRİLMESİ

Mekanik bağlantı elemanları ile birleştirilen kompozitler ciddi delaminasyon hasarına, birleşme bölgesinde stres yığılmasına ve ağırlık artışına neden olduğundan son zamanlarda kompozit malzemelerin yenilikçi yöntemler ile birleştirilmesi daha fazla önem kazanmıştır. Bu birleştirme yöntemleri delaminasyon hasarını engellediği gibi stresin eşit bir şekilde dağılmasını sağlar ve ciddi ağırlık artışına neden olmaz. Fakat yenilikçi yöntemler ile birleştirilen kompozit parçaların yüzeyinin modifiye edilmesi kritik öneme sahiptir.

Bu çalışmada, %10 ağırlık/hacimce PA 66 ve %1, %2 ve %3 ağırlık/hacimce rGO ilaveli elektro-eğrilmiş nanolifler ile karbon/epoksi prepreg kaplanarak birleşme yüzeyi modifiye edilmiştir. Kompozit plakalar 3 kat FM 300K film yapıştırıcı kullanılarak ikincil yapıştırma (secondary bonding) yöntemi ile sıcak preste birleştirilmiştir. Nanoliflerin morfolojik yapısı ve rGO'nun dispersiyonu SEM ile analiz edilmiştir. Nanoliflerin termal özellikleri DSC ile analiz edilmiştir. Modifiye edilmemiş prepreg ve nanolif ile modifiye edilmiş prepreg yüzeyinin hidrofilik ve hidrofobik özelliklerini tespit etmek için temas açısı ölçüm cihazı kullanılmıştır. En hidrofilik özellik %2 rGO ilaveli nanolif kaplı yüzeyde görülmüştür. Modifiye edilmiş ve edilmemiş kompozit plakaların mekanik özelliklerini incelemek için Tek Tesirli Bindirme Bağlantı (SLJ) ve Charpy Darbe testleri yapılmıştır. SLJ testi ve Charpy Darbe testi sonuçlarına göre yüzeyi %2 rGO ile modifiye edilen karbon/epoksi kompozit parçalarda sırasıyla %17.89 ve %30.59 oranında iyileşme görülmüştür.

# TABLE OF CONTENTS

LIST OF FIGURES .....	viii
LIST OF TABLES .....	xi
LIST OF SYMBOLS .....	xii
CHAPTER 1. INTRODUCTION .....	1
1.1. An Overview of Composite Materials .....	1
1.1.1. Carbon Fiber–Reinforced Polymer (CFRP) Composites.....	3
1.2. Bonding and Surface Treatment of Structural Fiber Reinforced Composite Structures.....	4
1.2.1. Adhesive Bonding of Composites.....	4
1.2.2. Failure Modes.....	6
1.2.3. Surface Treatment .....	7
1.2.3.1. Electrospinning Method .....	7
1.4. Objectives .....	11
CHAPTER 2. LITERATURE REVIEW .....	13
CHAPTER 3. MATERIALS AND METHODS .....	16
3.1. Materials.....	16
3.2. Preparation of Solutions Containing PA 66 and PA 66/rGO.....	16
3.3. Coating of Electrospun on Carbon Prepreg .....	18
3.4. Production and Joining of Composite Laminates by Hot Press Method.....	19
3.5. Characterization and Surface Analysis Techniques.....	20
3.5.1. Scanning Electron Microscopy (SEM) .....	20
3.5.2. Differential Scanning Calorimetry (DSC) .....	21
3.5.3. Contact Angle Analysis.....	21
3.6. Mechanical Characterization.....	21
3.6.1. Single Lap Joints Test (SLJ) .....	22

3.6.2. Charpy Impact Test .....	22
CHAPTER 4. RESULTS AND DISCUSSION.....	24
4.1. Morphological Analysis of Nanofibers.....	24
4.2. Differential Scanning Calorimetry (DSC) Analysis .....	27
4.3. Contact Angle Measurement Analysis.....	29
4.4. Single Lap Joints (SLJ) Test .....	36
4.5. Charpy Impact Test.....	45
CHAPTER 5. CONCLUSION .....	49
REFERENCES .....	52

## LIST OF FIGURES

<u>Figure</u>	<u>Page</u>
Figure 1. Illustration of the phases of composite materials. ....	1
Figure 2. Classification of composite materials.....	2
Figure 3. Manufacturing techniques for CFRP.....	3
Figure 4. Schematic diagram of the hot press.....	4
Figure 5. Schematic representation of adhesive bonding. ....	6
Figure 6. Failure modes .....	6
Figure 7. Schematic representation of the electrospinning process.....	8
Figure 8. Nanofiber formation by electrospinning .....	9
Figure 9. Parameters affecting the electrospinning method. ....	9
Figure 10. Schematic representation of the solution preparation step.....	17
Figure 11. Electrospinning experiment setup .....	18
Figure 12. Schematic representation of prepreg sequence. ....	19
Figure 13. Curing graph of prepregs.....	20
Figure 14. Curing graph of secondary bonding of composite plates.....	20
Figure 15. Single lap joints test specimen. ....	22
Figure 16. Charpy impact test specimen.....	23
Figure 17. SEM image and nanofiber diameter of nanofibers containing 10% wt/v PA66 .....	24
Figure 18. SEM images of a) 10% PA 66 +1% rGO, b) 10% PA 66 + 2% rGO, and c) 10% PA 66 + 3% rGO containing nanofibers.....	25
Figure 19. Image of dispersion of a) 10% PA 66 + 1% rGO, b) 10% PA 66 + 2% rGO, and c) 10% PA 66 + 3% rGO.....	26
Figure 20. SEM images of a) nanofibers coated on aluminum foil, b) nanofibers coated on aluminum foil and pressed c) coated on carbon/epoxy, and d) nanofiber coated on carbon/epoxy prepreg and cured plate. ....	26
Figure 21. DSC graphs of 10% PA 66 + 0% rGO .....	27
Figure 22. DSC graphs of 10% PA 66 + 1% rGO .....	28
Figure 23. DSC graphs of 10% PA 66 + 2% rGO .....	28
Figure 24. DSC graphs of 10% PA 66 + 3% rGO .....	29

<b><u>Figure</u></b>	<b><u>Page</u></b>
Figure 25. Images of the contact angle test measurements of the prepreg (without nanofibers) at 1st, 30th, and 60th seconds a)1 <sup>st</sup> sample b)2 <sup>nd</sup> sample c)3 <sup>rd</sup> sample.....	30
Figure 26. Images of contact angle test measurements of nanofibers containing 10% PA 66 + 0% rGO at 1st, 30th, and 60th seconds a)1 <sup>st</sup> sample b)2 <sup>nd</sup> sample c)3 <sup>rd</sup> sample .....	31
Figure 27. Images of contact angle test measurements of nanofibers containing 10% PA 66+ 1% rGO at 1st, 30th, and 60th seconds a)1 <sup>st</sup> sample b)2 <sup>nd</sup> sample c)3 <sup>rd</sup> sample .....	32
Figure 28. Images of contact angle test measurements of nanofibers containing 10% PA 66 + 2% rGO at 1st, 30th, and 60th seconds a)1 <sup>st</sup> sample b)2 <sup>nd</sup> sample c)3 <sup>rd</sup> sample .....	33
Figure 29. Images of contact angle test measurements of nanofibers containing 10% PA 66+ 3% rGO at 1st, 30th, and 60th seconds a)1 <sup>st</sup> sample b)2 <sup>nd</sup> sample c)3 <sup>rd</sup> sample .....	34
Figure 30. Image of a single lap joints test sample.....	36
Figure 31. The load-displacement curve of 0% PA 66 + 0% rGO (without nanofibers) composite plates.....	37
Figure 32. The load-displacement curve of 10% PA 66 + 0% rGO composite plates.....	38
Figure 33. The load-displacement curve of 10% PA 66 + 1% rGO composite plates.....	39
Figure 34. The load-displacement curve of 10% PA 66 + 2% rGO composite plates.....	40
Figure 35. The load-displacement curve of 10% PA 66 + 3% rGO composite plates.....	41
Figure 36. Average stress values of single lap joints test results.....	42
Figure 37. Before and after test images of single lap joints test specimens a) 0% PA 66 + %0 rGO (without nanofibers), b) 10% PA 66 + %0 rGO, c) 10% PA 66 + %1 rGO, d) 10% PA 66 + %2, rGO and, e) 10% PA 66 + %3 rGO. ....	43
Figure 38. Fracture surface images of single lap joints test specimens a) 0% PA 66 + %0 rGO (without nanofibers), b) 10% PA 66 + %0 rGO, c) 10% PA 66 + %1 rGO, d) 10% PA 66 + %2, rGO and, e) 10% PA 66 + %3 rGO .....	44
Figure 39. Image of the Charpy impact test sample .....	45
Figure 40. Average stress values of Charpy impact test results .....	46

<b><u>Figure</u></b>	<b><u>Page</u></b>
Figure 41. Before and after test images of Charpy impact test specimens a) 0% PA 66 + %0 rGO (without nanofibers), b) 10% PA 66 + %0 rGO, c) 10% PA 66 + % rGO, d) 10% PA 66 + %2, rGO and, e) 10% PA 66 + %3 rGO.. .....	47
Figure 42. Fracture surface images of Charpy impact test specimens a) 0% PA 66 + %0 rGO (without nanofibers), b) 10% PA 66 + %0 rGO, c) 10% PA 66 + %1 rGO, d) 10% PA 66 + %2, rGO and, e) 10% PA 66 + %3 rGO. ....	48

## LIST OF TABLES

<b><u>Table</u></b>	<b><u>Page</u></b>
Table 1. Advantages and disadvantages of mechanical fastening and adhesive bonding .....	6
Table 2. Contact angle measurements of prepregs and PA 66 and PA66/rGO nanofiber coated prepregs .....	34
Table 3. The average stress results of the single lap joints test. ....	42
Table 4. The Charpy impact test results. ....	46

# LIST OF SYMBOLS

## Nomenclature

a	Delamination Length [mm]
$a_{cN}$	Charpy Impact Strength [ $\text{kJ/m}^2$ ]
b	Specimen Width [mm]
$b_N$	Remaining Width of the Test Sample [mm]
$E_c$	Energy Absorbed by the Broken Test Specimen [J]
H	Thickness of the Test Specimen [mm]
$G_I$	Mode I Interlaminar Fracture Toughness [ $\text{kJ/m}^2$ ]
P	Load [N]

## Abbreviations

CFRP	Carbon Fiber–Reinforced Polymer
CM	Compression Molding
DCB	Double Cantilever Beam
FRP	Fiber Reinforced Polymers
IM	Injection Molding
PA 66	Polyamide 66
PCL	Polycaprolactone
PET	Polyethylene Terephthalate
rGO	Reduced Graphene Oxide
RTM	Resin Transfer Molding
SEM	Scanning Electron Microscopy
SLJ	Single Lap Joint
VARTM	Vacuum-Assisted Resin Transfer Molding
wt/v	Weight/volume

# CHAPTER 1

## INTRODUCTION

### 1.1. An Overview of Composite Materials

The word "Composite" comes from the French past participle of the verb "Componere", which means to put together, and comes from the Latin "Composites"[1]. Composite materials are obtained by combining two or more materials with different properties in a physical and macro structures under certain conditions and at specific rates to provide the desired properties without dissolving into each other. Composite materials consist of two primary phases: the matrix phase and the reinforcement phase. The matrix holds the fibers together, transfers the load on the material to the fibers, shapes the material, keeps the material rigid, and protects the material against environmental damage. The reinforcement element provides support to the matrix structure, carries a significant proportion of the incoming load, and increases the material volume[2]. The phases forming the composite materials are illustrated in Figure 1.



Figure 1. Illustration of the phases of composite materials.

The use of composite materials dates back to ancient times. People used animal or vegetable fibers to strengthen fragile materials. Examples of composite materials used in ancient times are particle boards made by Mesopotamians by combining wood chips and natural resin and adobe houses built by human beings for shelter. In the following periods, the bows obtained by the Mongols from plants, pine resin, and the tendons and horns of animals can be given as examples of the use of composite in history[3][4].

In the early 20th century, synthetic plastics such as bakelite, vinyl, polystyrene, phenolic, and polyester were developed. However, these resins were insufficient in terms of strength in some applications. In the 1930s, the Owen Corning Corporation introduced fiberglass. The necessity of reinforcing plastics in structural applications and the discovery of glass fiber were simultaneous. This development marked the beginning of the Fiber Reinforced Polymers (FRP) industry. This new material has been the focus of attention, especially in the aerospace industry. Because a different material has emerged, that will offer the features that the traditional material cannot provide. With the II. World War, the production of more aircraft increased the use of composites in structural parts. The beginning of the 1950s was the date when filament winding, pultrusion, and vacuum molding techniques were tried for the first time. Today, the development of composite materials continues[4], [5].

Monolithic traditional metal alloys, ceramics, and polymeric materials, which alone are insufficient to achieve the desired goal in many industries such as aviation, space, bioengineering, transportation, defense, and maritime, are replaced by composite materials. Composite materials can be classified according to the matrix phase and the reinforcement element [2], [6]. Classification of composite materials according to matrix and reinforcement phases is given in Figure 2.

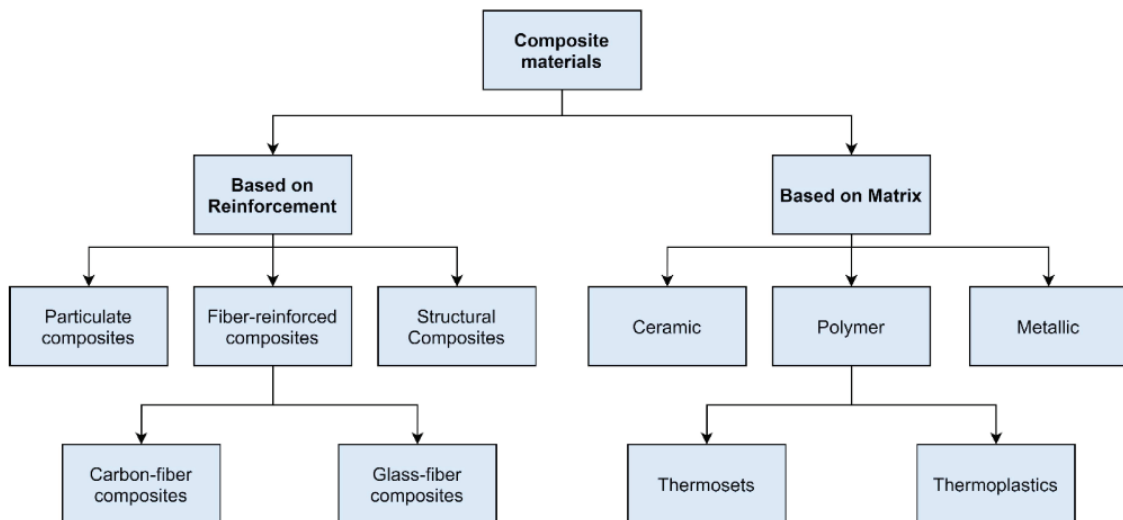


Figure 2. Classification of composite materials

(source: E. Shehab et al., 2023 [7]).

### 1.1.1. Carbon Fiber–Reinforced Polymer (CFRP) Composites

Composites in which carbon fiber is used as a reinforcing phase and a polymer matrix is used to hold the reinforcing elements together are called carbon fiber-reinforced polymer composites. CFRP materials have good stiffness, a high strength-to-weight ratio, corrosion resistance, vibration resistance, high fatigue resistance, and low thermal conductivity. Due to the advantages, it is used in aviation, automotive, maritime, etc. and can be used in many industries. Various methods are used to produce CFRP composites. In Figure 3, these production methods are classified[6].

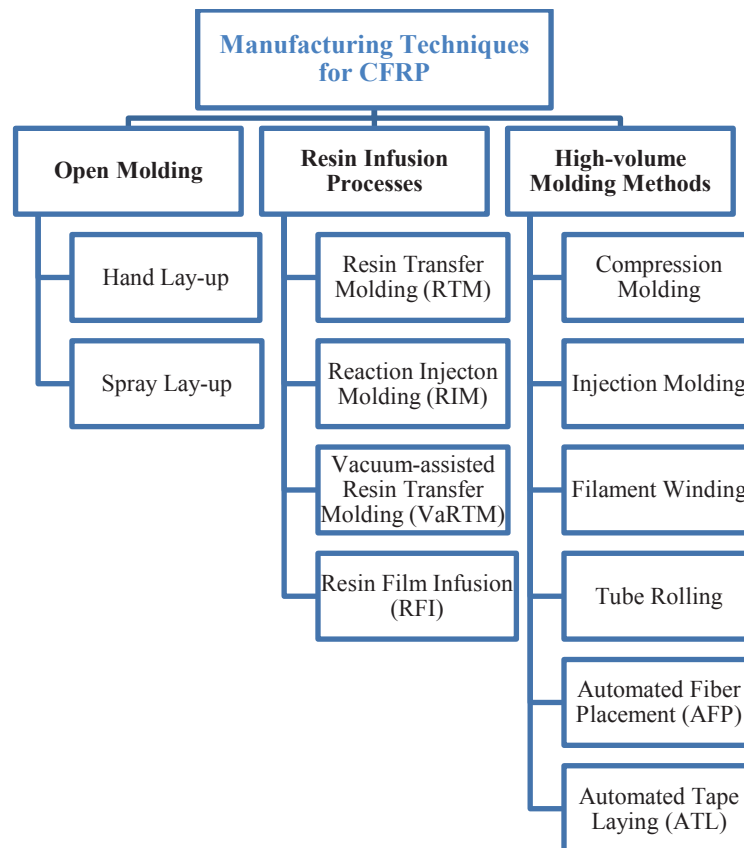


Figure 3. Manufacturing techniques for CFRP

(source: B. Beylergil, 2017 [4]).

Compression molding (CM) is one of the methods used to produce FRP. Female and male molds are mounted on a mechanical or hydraulic press. While the mold is open, the material is placed between the mold and produced under a suitable temperature and pressure to obtain the desired shape. The temperature and pressure of the mold are maintained until the material hardens, and after the mold is cooled, the product is removed

from the press. The compression molding method is schematized in Figure 4. Short cycle time, easy automation, high productivity and dimensional stability, good finished surface, and repeatability are the main advantages of this production method. It is also one of the low-cost molding technologies compared to other FRP production methods such as injection molding (IM), resin transfer molding (RTM), and vacuum-assisted resin transfer molding (VARTM)[8][9]. In this thesis study, composite plates were produced with a hydraulic hot press device, which is a compression molding method.

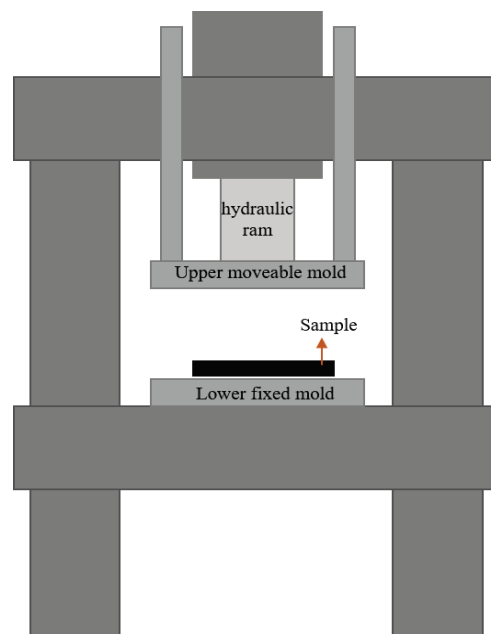


Figure 4. Schematic diagram of the hot press.

## 1.2. Bonding and Surface Treatment of Structural Fiber-Reinforced Composite Structures

### 1.2.1. Adhesive Bonding of Composites

Fiber-reinforced polymer (FRP) composite parts have been the focus of attention in the aerospace industry because of their strength and lightness. Therefore, the joining of fiber-reinforced composite parts has become a significant issue[10][11]. Conventionally used fasteners (screws, rivets, etc.) give rise to severe delamination, early crack initiation, and an increase in weight. Mechanical fasteners cause stress concentrations around the fastener and fiber damage. Adhesive bonding, which is another joining method, provides important advantages such as uniform stress distribution,

lightness, and high damage tolerance [12][13][14]. Table 1 shows the advantages and disadvantages of mechanical bonding and adhesive bonding methods.

Table 1. Advantages and disadvantages of mechanical fastening and adhesive bonding (source: N. Paranjpe, 2016 [12] and B. Reyhan Deniz Atay, 2019 [15]).

	<b>Advantages</b>	<b>Disadvantages</b>
<b>Mechanical Fastening</b>	<ul style="list-style-type: none"> <li>▪ No surface preparation is required</li> <li>▪ Possibility to disassemble and reassemble</li> </ul>	<ul style="list-style-type: none"> <li>▪ Increase the weight</li> <li>▪ Corrode easily</li> <li>▪ Causing stress concentration around the fastener</li> <li>▪ Adversely affects the radar-absorbing characteristics</li> </ul>
<b>Adhesive Bonding</b>	<ul style="list-style-type: none"> <li>• Lighter joints</li> <li>• Uniform stress distribution</li> <li>• Ease of design</li> <li>• Reduction in production cost</li> <li>• High tolerance to damage</li> </ul>	<ul style="list-style-type: none"> <li>• Surface preparation is required</li> <li>• The curing process increases the manufacturing process</li> <li>• Undetachable</li> <li>• Easy to be affected by environmental conditions such as temperature and humidity</li> </ul>

Adhesive bonding is broadly classified into three categories as co-curing, secondary bonding, and co-bonding. In Figure 5, the types of adhesive bonding are schematized. In the co-curing method, two uncured parts are bonded with or without adhesive simultaneously. There is a decrease in production time, labor cost, and energy consumption since the joining with the co-curing method takes place in a single cycle. In addition, this method is an advantage in terms of the structural performance of the part. However, it is quite difficult to combine large and complex composite structures by the co-curing method because huge production facilities are required. In this case, the secondary bonding method provides a significant advantage over the co-curing method. Because thanks to the secondary bonding method, two pre-cured rigid composites are joined using the adhesive. The co-bonding method includes co-curing and secondary bonding methods. With this technique, the cured rigid composite and the uncured prepreg are combined with the adhesive[11][16][17].

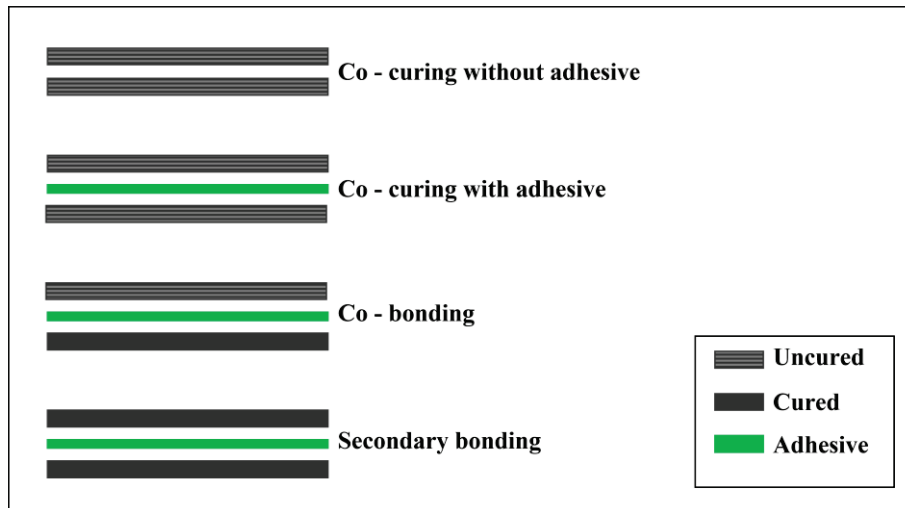


Figure 5. Schematic representation of adhesive bonding.

### 1.2.2. Failure Modes

Choosing a convenient joining method when joining composite parts is critical in terms of failure modes and joint strength [15]. Failure modes in adhesively bonded FRP joints are defined by ASTM D5573 Standard. Figure 6. shows the failure modes according to the ASTM D5573 Standard.

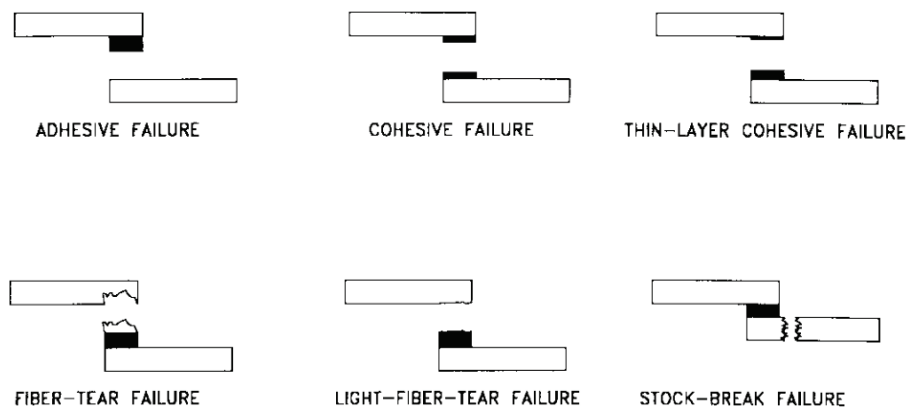


Figure 6. Failure modes

(source: ASTM D5573 standard [18]).

The failure modes seen in adhesive bonding can be defined by three basic failure modes as cohesive failure, adhesive failure, and adherent failure [15]. Adhesive failure can be recognized by the absence of any adhesive residue on one of the FRP surfaces [18].

This failure may indicate insufficient surface preparation before bonding. The presence of adhesive on both FRP surfaces is an indication of cohesive failure mode. This failure may be due to the adhesive notwithstanding the applied load or poor joint design. Adherent failure proves that the bonding method is not the weakest defect in the structure because the damage is observed in the adherent, not in the adhesive[15][18].

### **1.2.3. Surface Treatment**

Surface preparation is critical for the formation of a strong bond between the adherent and the adhesive in the composite parts bonded with the adhesive. Surface preparation is the process of cleaning the surface by physical or chemical means, increasing the surface area, and modifying the surface to ensure that the adhesive adheres well to the surface[19], [20].

#### **1.2.3.1. Electrospinning Method**

Nanofibers are used in many fields due to their small size, high surface area, high surface energy, and superior mechanical properties [21], [22]. Nanofibers are produced from a polymer solution or polymer melt in scales below micrometers [22]. The most common method used for the production of nanofibers from polymer solutions is the electrospinning method. The electrospinning experimental setup consists of three fundamental parts, namely the high-voltage power supply, the supply unit, and the collector[23], [24].

The electrospinning method is used to create nanofibers through an electric field. Firstly, the polymer solution obtained by dissolving it in the solvent is placed in the syringe. A high voltage is applied between the needle tip and the collector. The polymer drop suspended at the tip of the needle stays spherical due to the force created by the surface tension. With the applied high voltage, the surface charge of the polymer droplet increases, and the spherical droplet begins to take the shape of a cone by elongating, this is called a Taylor cone. When the surface charge exceeds the threshold value, that is, the surface tension of the polymer, the polymer solution creates a jet drawn towards the grounded collector, forming nanofibers on the collector [24]–[26]. The electrospinning process is shown in Figure 7.

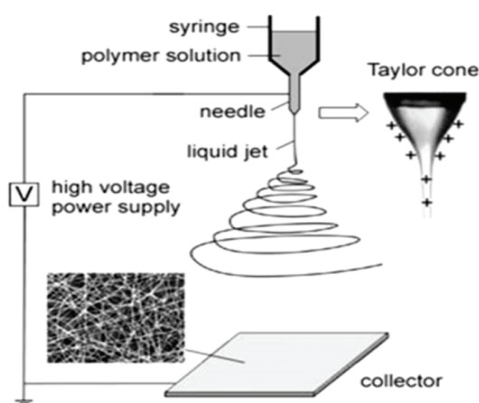


Figure 7. Schematic representation of the electrospinning process

(source: K. Garg et al., 2011 [24]).

While the jet is moving towards the collector, after leaving the Taylor cone, it moves for a certain period and then becomes unstable. Instability can take three forms. These instability states: i) classical Rayleigh instability, ii) Axisymmetric conducting instability, and iii) Whipping instability. The most common instability is whipping instability. Whipping instability occurs when the charges on the jet surface mutually repel each other and because the charges cannot be together, a radial torque is generated in the jet from the center. As the jet approaches the collector plate, small jets are formed as a result of the repulsion of the radial loads. The liquid jet is constantly elongated and thinner, and as a result of the evaporation of the solvent, the fibers at the micrometer level fall to the nanometer level, producing nano-sized fibers [21], [24], [27]. Figure 8 shows the formation of nanofibers by the electrospinning method.

Nanofibers with different structures can be obtained by using different polymer solutions in the electrospinning method. It is very important to obtain nanofibers with continuous, controllable pore size, controllable fiber diameter, high surface area/volume ratio, and bead-free or controllable bead ratio in nanofiber production [29]–[31]. The parameters affecting the nanofiber properties are examined in three groups. Parameters affecting nanofiber production are given in Figure 9.

In the electrospinning method, the molecular weight, viscosity, surface tension, conductivity, and dielectric constant of the solution affect the nanofiber properties.

The molecular weight of the polymer is related to the solution viscosity. The solution prepared with high molecular weight polymers also has a high viscosity [30]. High viscosity causes clogging of the needle tip or freezing of the solution at the needle tip. Also, the high-viscosity solution causes the fiber diameter to be thick. When the

viscosity of the solution is low, it causes the drop at the tip of the needle to fall to the ground under the effect of gravity. In addition, it accumulates in the collector in the form of spray, not in the form of fibers. Low viscosity also causes the formation of a bead structure on the nanofiber surface. The solution conductivity ensures that the nanofibers are bead-free and small in diameter. Because as the solution conductivity increases, the tension of the Taylor cone increases and so the jet tension rises. The realization of fiber production depends on the electrostatic forces exceeding the surface tension force. The low surface tension facilitates the electrospinning process. In addition, the high surface tension may cause the solvent molecules to come together and form a beaded structure on the nanofiber. The high dielectric constant of the solvent used reduces bead formation and results in fine nanofibers [23], [26], [30].

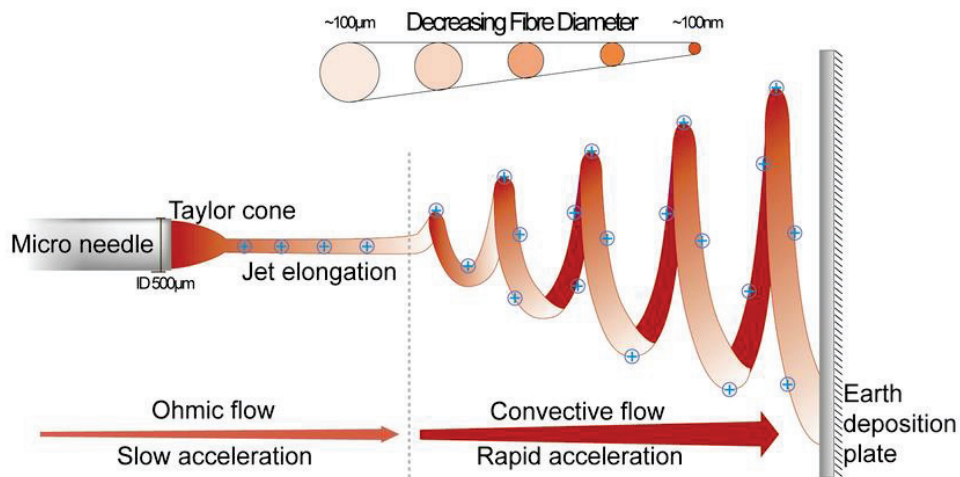


Figure 8. Nanofiber formation by electrospinning  
(source: O. Hardick et al., 2011 [28]).

Solution Parameters	Processing Parameters	Ambient Parameters
<ul style="list-style-type: none"> <li>• Molecular weight</li> <li>• Viscosity</li> <li>• Conductivity</li> <li>• Surface tension</li> <li>• Dielectric constant</li> </ul>	<ul style="list-style-type: none"> <li>• Applied voltage</li> <li>• Pumping speed</li> <li>• Solution temperature</li> <li>• Distance between needle tip to collector</li> <li>• Needle tip diameter</li> </ul>	<ul style="list-style-type: none"> <li>• Temperature</li> <li>• Humidity</li> <li>• Pressure</li> <li>• Atmosphere</li> </ul>

Figure 9. Parameters affecting the electrospinning method.

Process parameters such as voltage, pumping speed, solution temperature, needle, and collector distance, and needle tip diameter applied in nanofiber production by electrospinning are the factors affecting production.

The most basic parameter of the electrospinning process is high voltage. Thanks to the high voltage, the necessary load is provided to the solution to be affected by the electric field, and an electric field is formed between the needle tip and the collector. The critical value of the applied voltage varies according to the polymer solution. The applied voltage above this threshold causes the jet to move in the direction where the high voltage is applied. As the voltage is increased, more charge builds up on the solution, resulting in a faster jet. But this causes the Taylor cone to be unstable. During the process, high tension causes the load accumulated on the solution, so the repulsive force created by these loads also increases. In this case, the stretching of the jet increases, and finer fibers are formed [24], [26], [29], [31]. High tension also affects the crystal structure of nanofibers. The electric field causes the polymer molecules to line up more regularly. But it takes time for the polymer molecules to line up in a particular order, and that's when they go from the needle tip to the collector. If the voltage is too high, the time will be shortened and there will be insufficient time for crystallization [24]. Therefore, the voltage should neither be too low nor too high. The flow rate of the solution is a critical parameter for electrospinning and the critical value of this flow rate is the value at which the Taylor Cone is stable. When the flow rate exceeds this critical value, fiber diameter, and bead formation also increase [26], [32]. The solution temperature, on the other hand, affects the evaporation rate during the process and causes the viscosity to decrease. Thus, finer fibers can be obtained [29]. It is of great importance that the collector is a conductive material, as fiber production occurs thanks to the electric field formed between the needle tip and the collector. In addition, the distance between the needle tip and the collector is critical for the residence time of the fibers because the solution must evaporate before it reaches the collector. As the distance between the needle tip and the collector increases, the residence time of the fibers increases, but the intensity of the electric field decreases [23]. Another criterion is the needle tip diameter. The smaller the needle tip diameter, the finer fibers are produced [31].

The ambient parameters affecting the electrospinning method are temperature, humidity, pressure, and atmosphere. In fibers produced in a humid environment, porous fiber structure is seen due to the condensation of water molecules on the fiber. In addition, the evaporation rate of the solvent is higher in non-humid environments, and a more

uniform fiber structure is observed. Under low pressure, the tendency of the droplet to flow increases, and an unstable jet is formed. Electrical charges are easily discharged at very low pressure and electrospinning does not occur. The behavior of gases under an electric field differs. Therefore, the type of atmosphere is important during the electrospinning process [26], [29], [31].

The fact that there are many parameters affecting the electrospinning process makes the optimization of the parameters difficult. On the other hand, nanofibers produced by electrospinning are among the advantages of providing a wide application area, having controllable fiber diameter, having high production speed, low production cost, having high surface area, and is suitable for various modifications [29], [32], [33].

#### **1.4. Objectives**

The use of composite materials is increasing day by day due to the many advantages it provides. Especially in the aviation industry, fiber-reinforced structural composite parts are found promising with their superior strength, lightness, high corrosion, and fatigue resistance. With fiber-reinforced structural composite parts being the focus of attention, the joining of these parts has also become a point of interest. Fiber-reinforced composite parts joined by conventional methods cause serious problems such as weight gain, delamination, and stress accumulation around the fastener. In addition, these metallic joining elements such as screws and rivets cause corrosion and adversely affect electromagnetic properties. For this reason, the use of film adhesives, which is one of the innovative bonding techniques, is increasing. However, surface modification is required for this bonding technique.

In the present study, the carbon/epoxy prepreg used in the junction area was coated with PA 66 and PA 66/rGO electrospun nanofibers and the surface was modified. The prepreps were produced by the hot press method and bonded with the secondary bonding method in the hot press using 3 plies of FM 300K film adhesive. The main aim of the study is to increase the mechanical performance by modifying the bonding surface of fiber-reinforced composite parts with graphene-added electrospun nanofibers by using film adhesive instead of traditional fasteners that increase weight and cause delamination. Therefore, by increasing the surface area with PA 66 nanofibers, better adhesion of the adhesive to the surface is ensured and the mechanical properties are further improved

with the addition of rGO. A solution was prepared by dissolving 10% by weight/volume PA 66 pellets in formic acid and chloroform (75:25 volume/volume ratio, respectively) to form nanofibers by electrospinning, and 1%, 2%, and 3% w/v to further increase the mechanical properties. rGO was dispersed into the solution. SEM analysis was used to examine the morphological structure of nanofibers and the dispersion of rGO in the nanofiber network. The thermal properties of nanofibers were analyzed by DSC. Contact angle tests were performed to investigate the adhesion behavior of the adhesive to the surface and to explore the hydrophilic or hydrophobic properties of the surface. Single Lap Joints (SLJ), and Charpy Impact tests were performed to examine the mechanical property characterization.

## CHAPTER 2

### LITERATURE REVIEW

There is a rising interest in composite material research since it has become more inevitable to use, especially in aviation and wind turbine manufacturing. The utilization of composite materials adds value to the production process via higher strength and lower weight, reduction in manufacturing time, and safety risks. The advantages, such as strong corrosive resistance, being lighter, and superior fatigue strength, make prepreg fabrics promising when compared to widely used other materials like metals. Another point as crucial as composite materials is to find alternative techniques to reduce the utilization of some commonly used components like screws and rivets since they tend to absorb stress. They pose additional weight increases and affect the structure adversely via insufficient delamination and corrosion problems. Therefore, recent publications in the literature concentrate on new bonding techniques such as co-curing, co-bonding, and secondary bonding instead of commonly applied mechanical fasteners.

Kweon et al.[34] tested the double lap joints of composite and aluminum parts with adhesive, bolt and hybrid (bolt-adhesive) joining. they used film adhesive and paste adhesive for joining. According to the results, the bolted joint performed better than the paste adhesive, while the film adhesives also performed better than the bolted joint. On the other hand, in hybrid bonding, film adhesive and bolted joints did not have much effect on strength, while the samples joined with bolt and paste adhesive showed better strength than bolt and paste adhesive joints. Kim et al.[13] tested single lap joints test unidirectional composites which bonded with secondary bonding and co-curing (with or without adhesive) methods. The samples joined by co-curing method without adhesive showed the highest failure strength. However, the samples bonded with the adhesive by co-curing method showed lower failure strength than the samples bonded with the secondary bonding method. Wu et al.[11] designed the mold to optimize the adhesive thickness by examining the shear strength of the composite parts joined by the secondary bonding method. With the mold designed according to the results, the adhesive thickness was optimized and the shear strength was improved compared to the traditional bonding method. In the study of Song et al.[35], four distinct bonding techniques, which are co-curing w/wo adhesive, co-bonding, and secondary bonding, are applied to get single lap

joint samples. The test results show that the samples produced by co-curing and secondary bonding techniques have higher strength while the performance of the co-bonding technique falls behind.

In the adhesive bonding method, surface modification is required for the adhesive to bond strongly to the surface. It is known in the literature that nanofibers increase mechanical performance and are also used in surface modification.

Sanatgar et al.[36] investigated how formic acid and formic acid/chloroform (3/1) as solvents with different solution concentrations will affect solid-state polymerized PA 66 by using the electrospinning technique. The authors implied that the concentration of solution plays a key role in the modulus of electrospun nanofibers. Moreover, the mixing of formic acid and chloroform dramatically impacts crystallinity. The results show that if 10 wt. % chloroform is included in the solution of PA 66 with formic acid, crystallinity rises 51.2% in comparison to the case without chloroform. Beylergil et al.[37] interspersed polyamide 66 nanofibers with 17 gsm and 50 gsm density on carbon reinforced polymer composites. PA 66 nanofibers resulted in a significant increase in initial and propagation mode-I fracture toughness. In addition, improvements were observed in Charpy impact strength. Brugo and Palazzetti[38] interspersed nylon 6,6 nanofibers of two different thicknesses into unidirectional and plain wave carbon/epoxy composites. They examined the effect of fabric type and nanofiber thickness by applying fracture loads of modes I and II and showed that fabric nature and nanofiber thickness had an effect on the results. Daelemans et al.[39] investigated mode-I and mode-II fracture toughness by interspersing polyamide 6.6 and polyamide 6.9 nanofiber veils on carbon/epoxy composite. As a result, they determined an increase in  $G_{IC}$  and  $G_{IIC}$  values. They reported that nanofibers affect the toughening mechanism by bridging the microcracks formed in the part.

Parlayıcı et al.[40] obtained and characterized nylon-6.6 (N6.6)/graphene oxide (GO) nanofibers. To add GO nanofiber structure, they were synthesized by Hummer's method. To add GO to N6,6, they first dissolved the N6,6 pellets in formic acid. Then, GO was added to chloroform and dispersed with a sonicator for 10 minutes. Finally, the two prepared solutions (N6,6/formic acid and GO/chloroform) were mixed in a sonicator for 1 hour. Maccaferri et al.[41] added graphene in different rates to the Nylon 66 nanofibers. They found that the addition of graphene did not affect the thermal properties, but the addition of graphene did affect the nano diameter. Kim et al. [42] produced PA 66 nanocarbon composites by adding a hybrid filler (graphene oxide and multi-walled

carbon nanotube) to the polymer matrix. According to the results, improvements were observed in Young's modulus, yield stress and tensile strength. Cakal Sarac et al.[43] characterized the nanocomposites and investigated their mechanical properties by adding a single layer of amine functionalized reduced graphene oxide and multilayer thermally exfoliated graphene oxide (TEGO) to PA 66 nanofibers. As a result, they reported that both graphene additions acted as a nucleating agent and TEGO showed a better tensile strength. In addition, the viscoelastic behavior of TEGO added nanocomposites is more stable.

Mohan et al.[44] conducted an experimental work to examine the effects of nanofibers produced by electrospinning and Al<sub>2</sub>O<sub>3</sub> nanoparticles on the toughness of mixed-mode fracture. Based on the test results, the authors observed cohesive and adhesive breakage in samples joined by secondary bonding and co-curing techniques, respectively, and reported that Mode II fracture has a higher toughness in comparison to Mode I. The addition of nanofills to the resin can enhance Mode I fracture toughness making resin more viscous, which is not desired since composite production may become problematic. There are various studies aiming to enhance the interleaving method in the interlayer region. According to the study of Van der Heijden et al.[45], Polycaprolactone (PCL) nanofiber among the applied porous structures leads to an almost 100 percent enhancement in the interlaminar fracture toughness. Similarly, Saz-orozco et al.[46] tried to find an answer how to enhance the Mode I fracture toughness in which polyamide (PA) and polyethylene terephthalate (PET) are used as interleaving materials. The SEM analysis demonstrated that performance of PA cover is greater via fiber bridging effect. PA 66 is a prominent thermoplastic material with its superior features: easy processability, compliance to uncured resin thanks to high phase change temperature, tendency to fiber-forming, reluctance to moisture absorption. In the study of Beckermann and Pickering[47], among different polymer types, 4.5 g/m<sup>2</sup> PA66 cover has a better laminate performance in terms of fracture toughness, Mode I:156%, Mode II:69%. Esenoglu et al [48]. investigated the morphological structure of nanofibers by adding PA 66 pellets to the solution at different rates. In addition, the mechanical properties of composite parts joined with PA 66 nanofibers by secondary bonding method were investigated. They used 2 plies and 3 plies FM 300K film adhesive in their work. The best single lap shear strength was seen in the composite samples whose bonding surface was improved with PA 66 nanofibers at a ratio of 10% wt. using 3 plies FM 300K.

## CHAPTER 3

### MATERIALS AND METHODS

#### 3.1. Materials

“HEXPLY M91/34%/UD194/IM7-12K” carbon/epoxy prepreg was used in this study. This prepreg used has a weight of  $294 \text{ g/m}^2$ , theoretically calculated at 59.2% fiber volume,  $1.28 \text{ g/m}^3$  resin density, and  $1.78 \text{ g/m}^3$  fiber density. In addition, the ply thickness calculated theoretically after curing is 0.184 mm [49].

Cytec FM 300K film adhesive was used to join the composite plates. This adhesive has a weight of  $244 \text{ g/m}^2$ , a thickness of 0.2 mm, and a green color. The FM300K film adhesive has a wide-open knit carrier. The prepreg and film adhesive used in the study were supplied by Turkish Aerospace Industries Inc [50].

Polyamide 6,6 pellets with Sigma Aldrich brand product code 429171 were used to produce nanofibers containing polyamide 6,6. The color is like off-white. Water content is less than or equal to 0.06% [51]. Formic acid (product code - 27001) and chloroform (product code - 24216) used as solvents are Sigma Aldrich brands. Nanografi brand with product code NG01RGO0101 reduced graphene oxide (rGO) was used. rGO is in the form of black powder and has a thickness of 0.5-2 nm, a width of 1-5  $\mu\text{m}$ , 2-5 layers, and a specific surface area of  $1562 \text{ m}^2/\text{g}$  [52]. Tekkim Teksoll brand Extra pure Ethyl Alcohol 96% + 2-Propanol mixture was used for surface cleaning.

#### 3.2. Preparation of Solutions Containing PA 66 and PA 66/rGO

The study of Esenoğlu et al [48]. is based on the solution preparation process and the use of 10% wt/v PA 66 pellets. To prepare PA 66 electrospun nanofibers, 10 g of PA 66 (polyamide 66) pellets were dissolved in 100 mL of formic acid/chloroform (75:25 v / v) with a magnetic stirrer at 300 rpm at room temperature for 12 hours and 10% PA 66 wt/v solution was prepared. PA 66 pellets were oven dried at  $80^\circ\text{C}$  for 24 hours before the solution was prepared. The solution was left in an ultrasonic bath for 10 minutes to remove air bubbles.

To disperse the graphene in solution, the work of Parlayıcı et al [40]. is based. The solution is dissolved in formic acid (56.25 ml) at 300 rpm for 12 hours by adding PA 66 pellets (7.5 g) after drying at 80°C for 24 hours. A solution is prepared with three different parameters (1%, 2%, and 3% wt/v rGO) by adding 0.75 g, 1.5 g, and 2.25 g rGO into chloroform (18.75 ml) in a separate beaker. rGO is dispersed in chloroform for 10 minutes with a QSONICA brand sonicator at a frequency of 500 watts, 20 kHz at 25% amplitude for 10 minutes. Then, two solutions containing Formic acid - PA 66 and chloroform - rGO are dispersed with a sonicator for 1 hour at 500 watts, 20 kHz frequency, and 50% amplitude. As the probe heats up with the operation of the sonicator, the solution is prepared in an ice bath. In addition, the mouth of the beaker is covered with parafilm to prevent gas escape. Solution preparation steps are schematized in Figure 10.

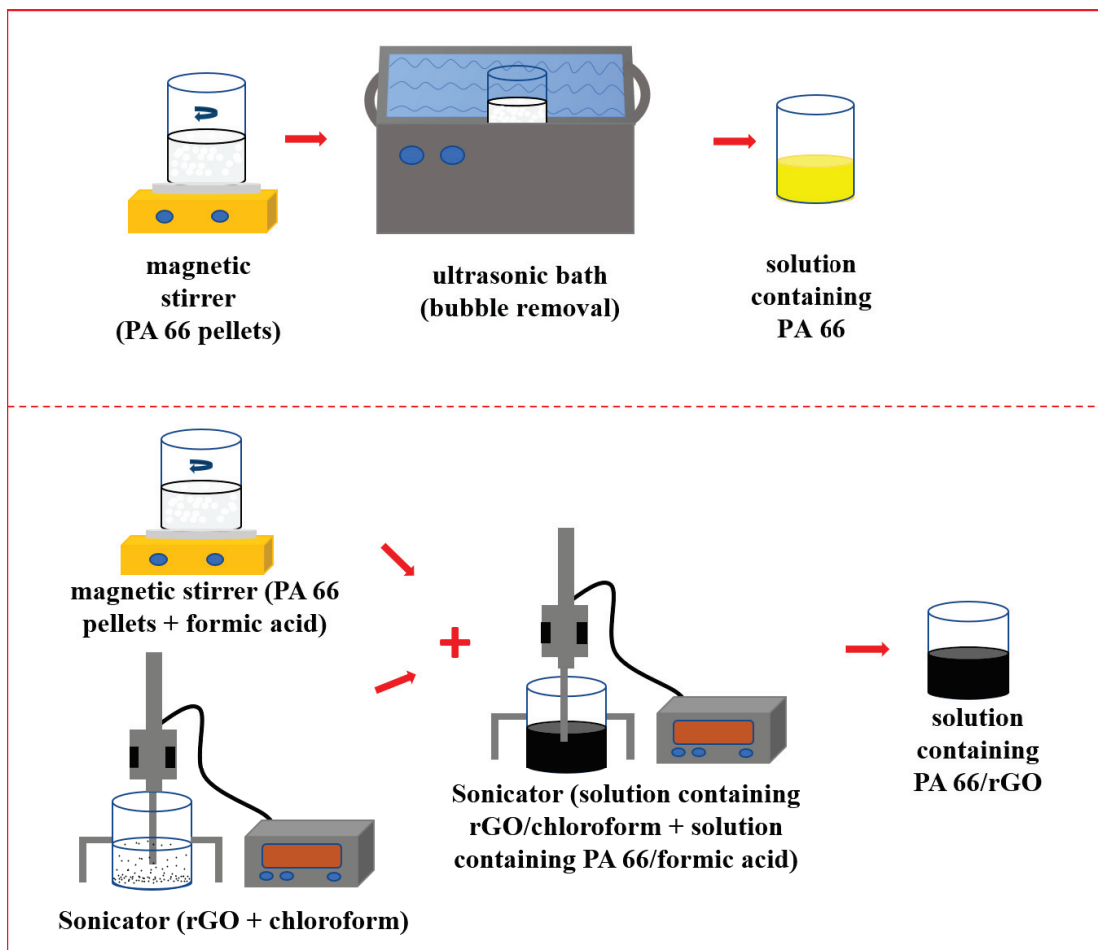


Figure 10. Schematic representation of the solution preparation step.

### 3.3. Coating of Electrospun on Carbon Prepreg

In this study, Inovenso PE-300 electrospinning device was used to coat carbon prepregs with nanofibers. The device provides advantages in production as it has 18 nozzles that can work at the same time, can move in the z direction providing homogeneity, has adjustable winding speed, has 2 programmable syringe pumps, and has 2 high voltage power supplies. Figure 11 shows the experimental setup of the electrospinning device.

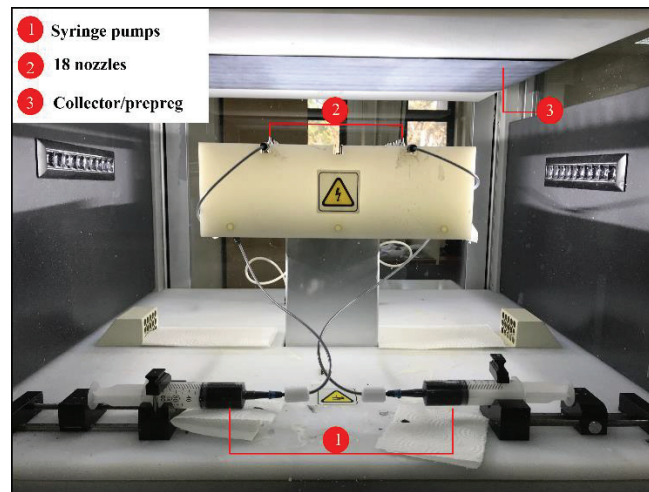


Figure 11. Electrospinning experiment setup

The parameters of the electrospinning device were determined based on the work of Esenoğlu et al [48]. 50 ml of the solution was filled into both syringes. The pumping speed of the syringes is 20ml/hr. 18 nozzles work simultaneously and nanofibers are produced with a 30 kV high-voltage power supply. For homogeneous coating of the prepregs with nanofibers, the collector moves in the z direction at a speed of 20 mm/s. The prepreg winding speed was set to 0.1 m/min and the spinning distance was 120 mm. The coating is adjusted on the touch screen of the device and makes 10 winding movements.

### 3.4. Production and Joining of Composite Laminates by Hot Press Method

Unidirectional carbon/epoxy preregs are laid in 12 layers as  $[45/-45/45/0/-45/90]_s$ . The prepreg containing PA 66 and PA 66/rGO nanofibers is cut at an angle of  $45^\circ$  and is located only in the joint region (top layer) of the produced plate. In Figure 12, the sequence of the preregs is schematized.

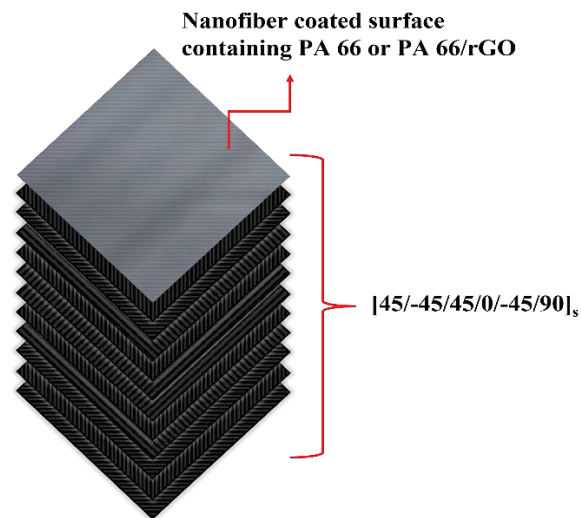


Figure 12. Schematic representation of prepreg sequence.

Prepregs containing PA66 and PA66+rGO nanofibers in the junction area were stacked on  $[45/-45/45/0/-45/90]_s$  and cured first at  $135^\circ\text{C}$  for 2 hours and then at  $180^\circ\text{C}$  for 2 hours and under 7 bar pressure. Kapton film is placed on the lower and upper surfaces of the prepregs to prevent them from sticking to the mold and any contamination on the surface. A mold release agent (Frekote 700-NC) was also applied to the Kapton films to prevent them from sticking to the mold. The curing graph of the prepregs containing PA 66 and PA 66/rGO nanofibers is given in Figure 13.

Composite plates coated with nanofibers in the joint area are joined in a hot press device using 3 plies (0.6 mm) FM 300K film adhesive with the secondary bonding method. The joining process is carried out in the hot press device under  $180^\circ\text{C}$  and 3 bar pressure for 120 minutes. Figure 14 shows the curing graph in which the plates are joined.

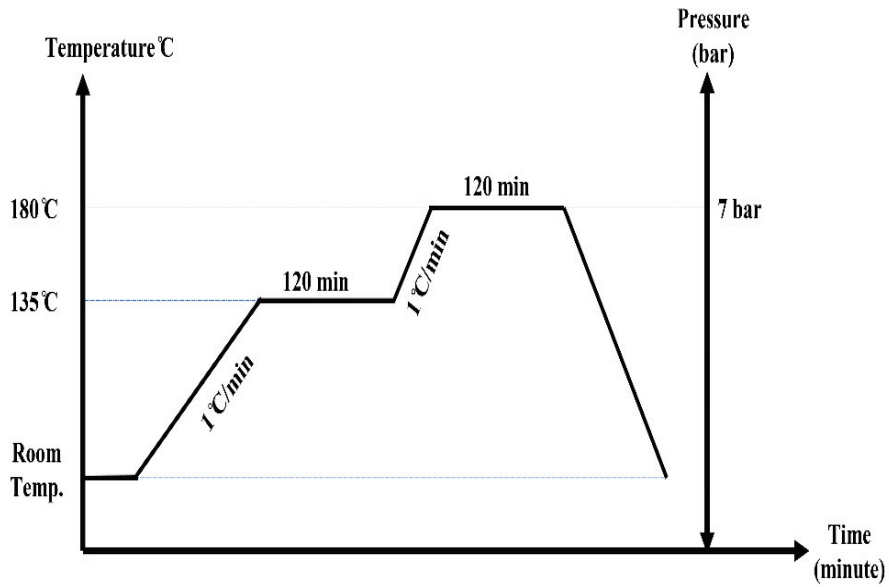


Figure 13. Curing graph of prepregs.

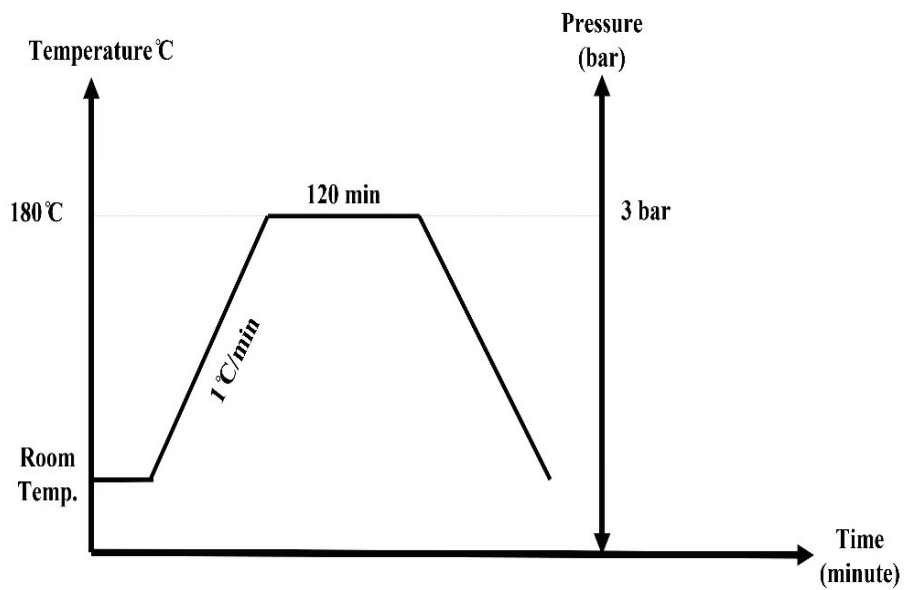


Figure 14. Curing graph of secondary bonding of composite plates.

### 3.5. Characterization and Surface Analysis Techniques

#### 3.5.1. Scanning Electron Microscopy (SEM)

The Scanning Electron Microscope (SEM) focuses a beam of electrons accelerated by a high voltage on the sample and takes an image by scanning the surface. Electrons interact with atoms in the sample and signals are formed. These signals reach

the relevant detector and give a micro and nano-size image of the structure on the surface of the material. In this study, the FEI QUANTA 250 FEG branded SEM device in IZTECH Center for Materials Research was used to examine the morphological properties of nanofibers and rGO added to the interlayers of nanofibers.

### **3.5.2. Differential Scanning Calorimetry (DSC)**

Differential Scanning Calorimetry (DSC) is a thermal analysis technique that measures the amount of energy absorbed or released from a material by heating, cooling, or keeping it at a constant temperature. With this technique, information about the material's thermal properties such as melting temperature, glass transition temperature, and phase change can be obtained. PERKIN ELMER – DSC 6000 brand DSC device located in the IZTECH Center for Materials Research

### **3.5.3. Contact Angle Analysis**

The contact angle measuring device records the images of the liquid dripped onto the material surface and analyzes the shape and contact angle of the drop on the surface over time. In this way, it provides information about the material surface such as contact angle, surface tension, wettability, and liquid spread. The contact angle was measured with a KSV Attension brand Theta model contact angle measuring device to examine the wettability of nanofibers.

## **3.6. Mechanical Characterization**

All mechanical test coupons were prepared by cutting in a wet cutting machine in accordance with the test standards. Before the samples were prepared, the edges of the composite plates were cut by approximately 20 mm. Preparing the test coupons from the middle of the composite plate ensured that they were prepared more homogeneously and realistically. The coupons, whose cutting process was completed, were dried in an oven at 60°C for 1 hour.

### 3.6.1. Single Lap Joints Test (SLJ)

Modified and unmodified carbon plates in the joint area were bonded with FM 300K film adhesive. The Single Lap Joints Test was applied to determine the shear strength of the adhesive. Tests were carried out using the MTS Landmark Servohydraulic Test System in the IZTECH laboratory. Test coupons were prepared according to ASTM D5868-01 standard. The test was carried out at a speed of 13 mm/min. Figure 15 shows the dimensions of the Single Lap Joints Test sample.

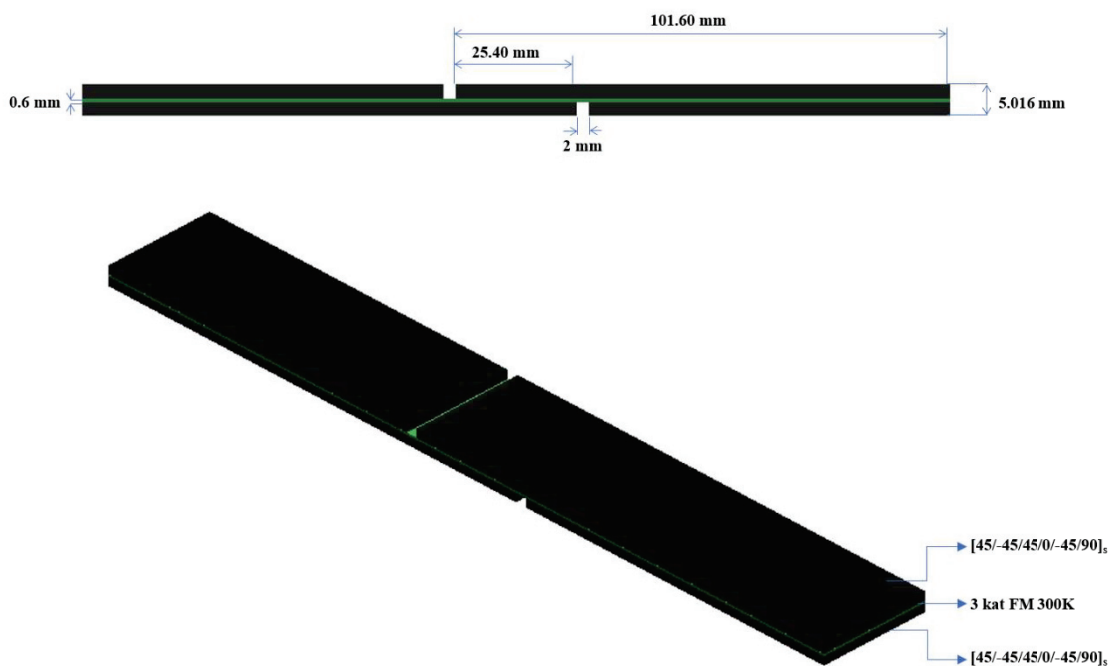


Figure 15. Single lap joints test specimen.

The load-displacement graph is obtained with the single-lap joints test. The shear strength value is calculated by dividing the maximum load obtained from the graph by the joint area. After the test, the joint area is examined and failure types are determined.

### 3.6.2. Charpy Impact Test

The Charpy-Impact test determines the impact strength of the material by measuring the amount of energy that the material can absorb. The samples were prepared according to the ISO-179 standard and V-notch (V-shaped notch) was opened on the

samples. The tests were carried out on the CEAST Resil Impactor device in the IZTECH laboratory. The potential energy of the hammer used is 15 Joules and its tangential speed is 3.46 m/s. Figure 16 shows the dimensions of the Charpy Impact Test sample.

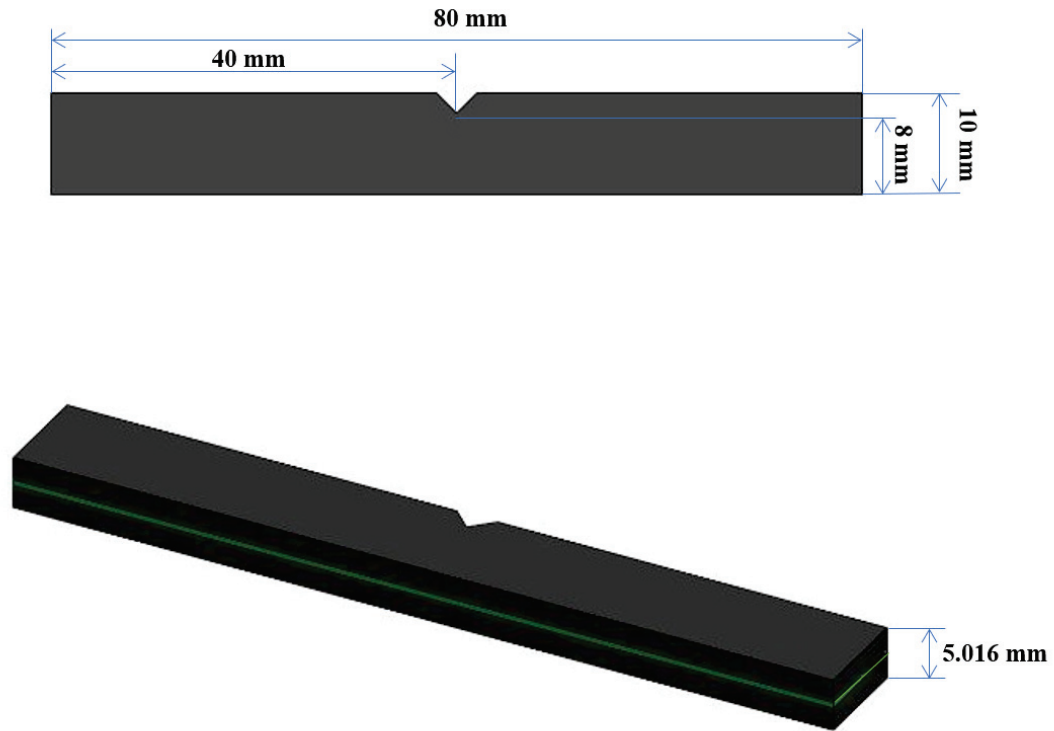


Figure 16. Charpy impact test specimen

The following equation is used to calculate the Charpy impact strength ( $a_{cN}$ ) for notched specimens.

$$a_{cN} = \frac{E_c}{hb_N} \times 10^3 \quad (\text{kJ/mm}^2) \quad (1)$$

$E_c$ : energy absorbed by the broken test specimen (joules),

$h$ : thickness of the test specimen (millimeters),

$b_N$ : remaining width of the test sample (millimeters).

## CHAPTER 4

### RESULTS AND DISCUSSION

#### 4.1. Morphological Analysis of Nanofibers

PA 66 nanofibers and reduced graphene oxide-added PA 66/rGO nanofibers were coated on carbon/epoxy prepreg with 45° fiber orientation. SEM image and nanofiber diameter of 10% wt/v PA 66 nanofibers are shown in Figure 17. The average value of 12 nanofiber diameters is (44.08 nm±13.06). When the structure of nanofibers is examined, beadless, uniform and thin nanofiber structure is seen.

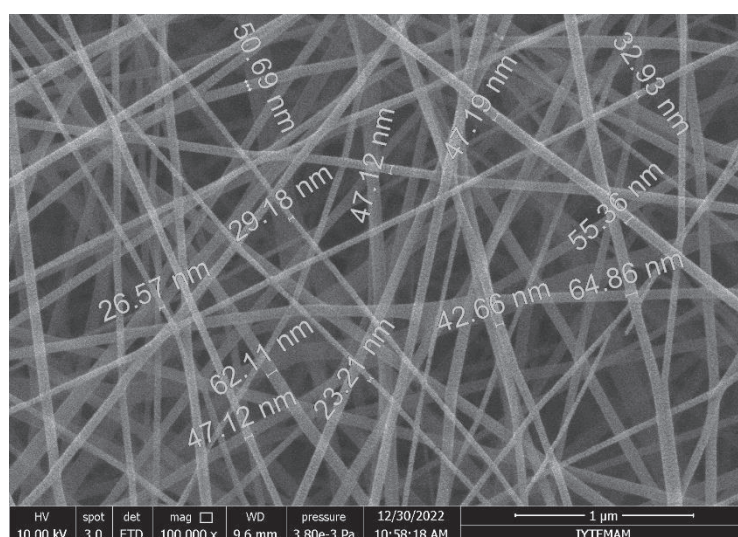


Figure 17. SEM image and nanofiber diameter of nanofibers containing 10% wt/v PA66

Reduced graphene oxide was added to the structure of nanofibers to further increase the bond strength. Figures 18.a, b, and c show the structure of rGO added to 10% PA 66 nanofibers at 1%, 2%, and 3% wt/v ratios, respectively. When the technical properties of the graphene used were examined, it was determined that the width of the graphene was between 1-5 µm. When the SEM images are examined, it is seen that the graphene widths of 1%, 2% and 3% are 5,720 µm, 5,348 µm, and 5,316 µm, respectively. In Figure 18.d, it is seen that graphene layers containing 3% rGO overlap in the structure of PA 66 nanofibers.

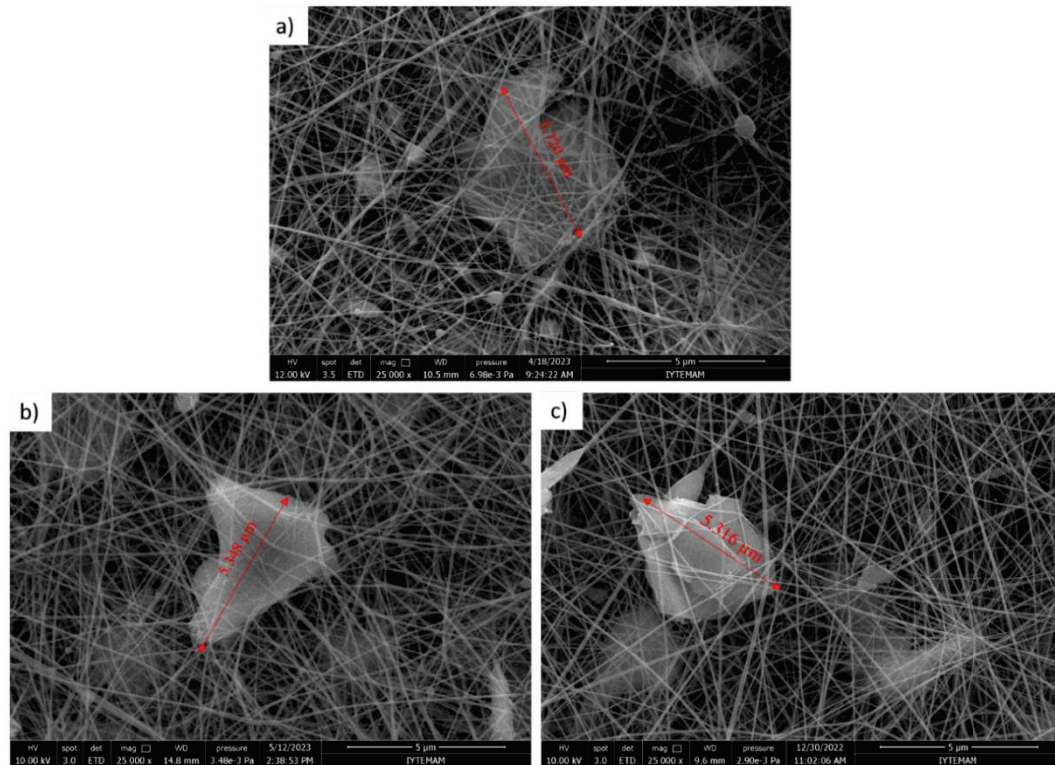


Figure 18. SEM images of a) 10% PA 66 +1% rGO, b) 10% PA 66 + 2% rGO, and c) 10% PA 66 + 3% rGO containing nanofibers

The dispersion of rGO added to PA 66 nanofibers is critical. In addition, determining the optimum ratio to be added is of great importance for the improvement of mechanical properties. Graphene tends to agglomerate, so its dispersion is important and difficult. Figure 19 shows that a) 1% rGO, b) 2% rGO, and c) 3% rGO are dispersed and rGO becomes more concentrated as the percentage increases.

After the nanofibers are coated on the prepreg, they are turned into composite plates in the hot press. To determine whether the nanofibers were damaged in the press, 10% PA 66 nanofibers were coated on the aluminum foil. Because it was predicted that nanofibers would not react with aluminum foil. The SEM image of the coating of 10% PA 66 nanofibers on aluminum foil is shown in Figure 20.a. In Figure 20.b, after 10% PA 66 nanofibers were coated on aluminum foil, they were first pressed at 135°C for 2 hours and then at 180°C for 2 hours under 7 bar pressure in a hot press. After the pressing process, it is seen that the nanofibers react between the neighboring chains. It is clearly seen in the figure that the mobility decreases as the nanofibers bond with each other. In Figure 20.c, SEM image of the coating of 10% PA 66 nanofibers on carbon/epoxy prepreg is given. In Figure 4.4.d, SEM image of the plate cured in a hot press under 7 bar pressure, first at 135°C for 2 hours and then at 180°C for 2 hours after 10% PA 66 nanofibers were

coated on carbon/epoxy prepreg. In Figure 20.d, it was determined that the nanofibers reacted with the epoxy and embedded in the epoxy.

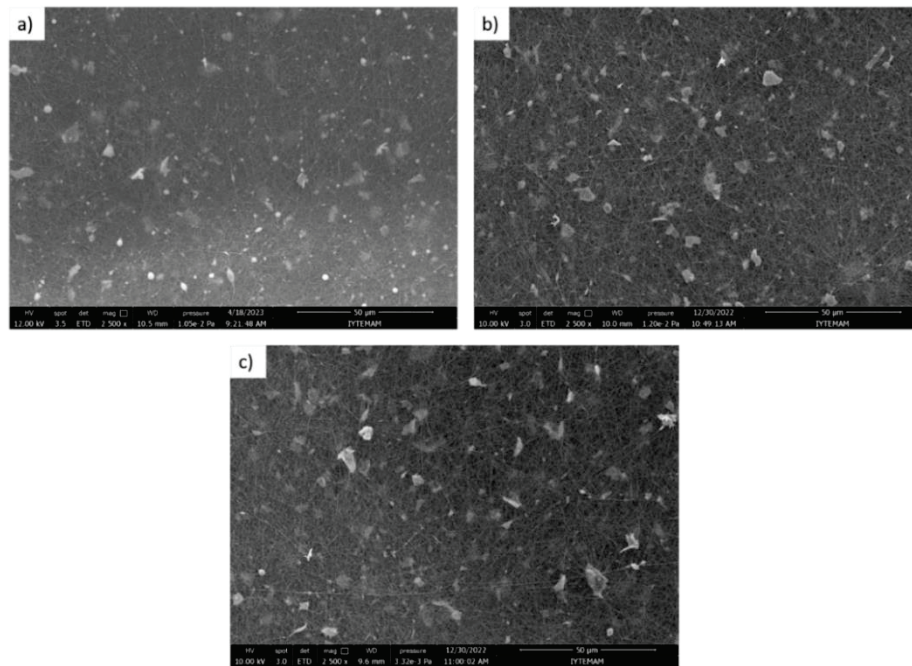


Figure 19. Image of dispersion of a) 10% PA 66 + 1% rGO, b) 10% PA 66 + 2% rGO, and c) 10% PA 66 + 3% rGO.

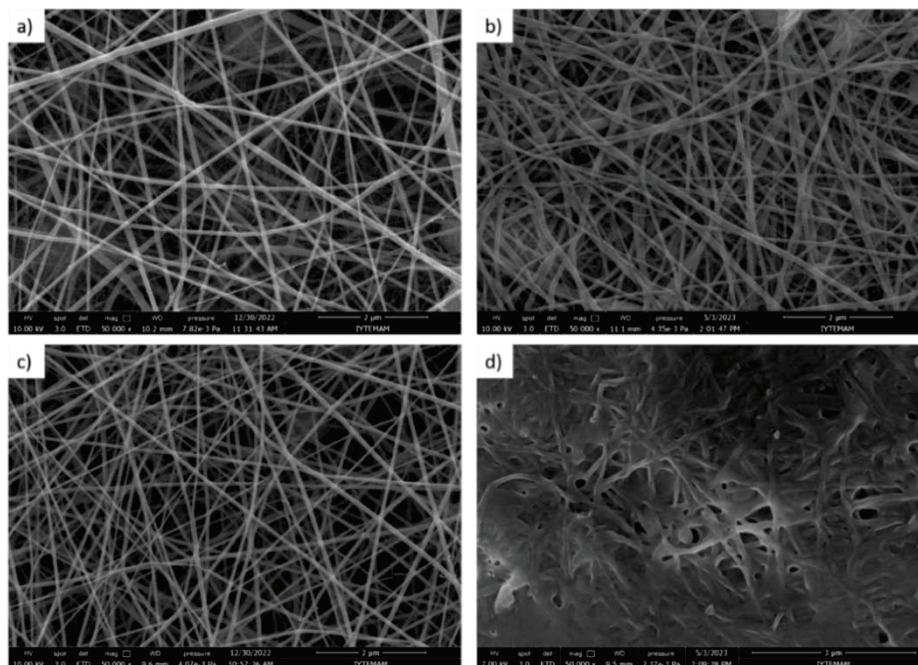


Figure 20. SEM images of a) nanofibers coated on aluminum foil, b) nanofibers coated on aluminum foil and pressed c) coated on carbon/epoxy, and d) nanofiber coated on carbon/epoxy prepreg and cured plate.

## 4.2. Differential Scanning Calorimetry (DSC) Analysis

DSC analysis were investigated to examine the thermal history of nanofibers. PA 66 and PA 66/rGO nanofibers were increased from 25°C to 300°C under nitrogen gas at a rate of 20°C/min. It was then cooled from 300°C to 25°C and again heated to 300°C from 25°C. In Figure 21. PA 66 nanofibers without rGO peaked at 265.38°C during the first heating. It peaked at 226.63°C when cooled and peaked at 250.16°C and 259.46°C when reheated. In Figure 22, when the DSC graph of 1% wt/v added rGO nanofibers was examined, peaks of 255.76°C and 266.11°C were observed in the first heating. When the cooling curve was examined, a peak of 230.58°C is observed. In the second heating curve, peaks were observed at 251.48°C and 261.88°C. In Figure 23, a peak was observed at 258.78°C and 266.44 °C in the first heating curve of nanofibers added with 2% wt/v rate of rGO, while a peak was observed at 232.88°C in the cooling curve. When the nanofibers were reheated, peaks were observed at 250.59°C and 258.17°C. Nanofibers added with 3% w/v rGO showed peaks at 248.50°C and 267.150°C in the first heating curve. It peaked at 231.49°C in cooling and 250.88°C and 261.58°C in reheating in Figure 24. It is seen that the addition of rGO to the nanofibers in the first and second heating did not affect the melting temperature. When the cooling curves are examined, it is seen that the addition of graphene accelerates the crystallization.

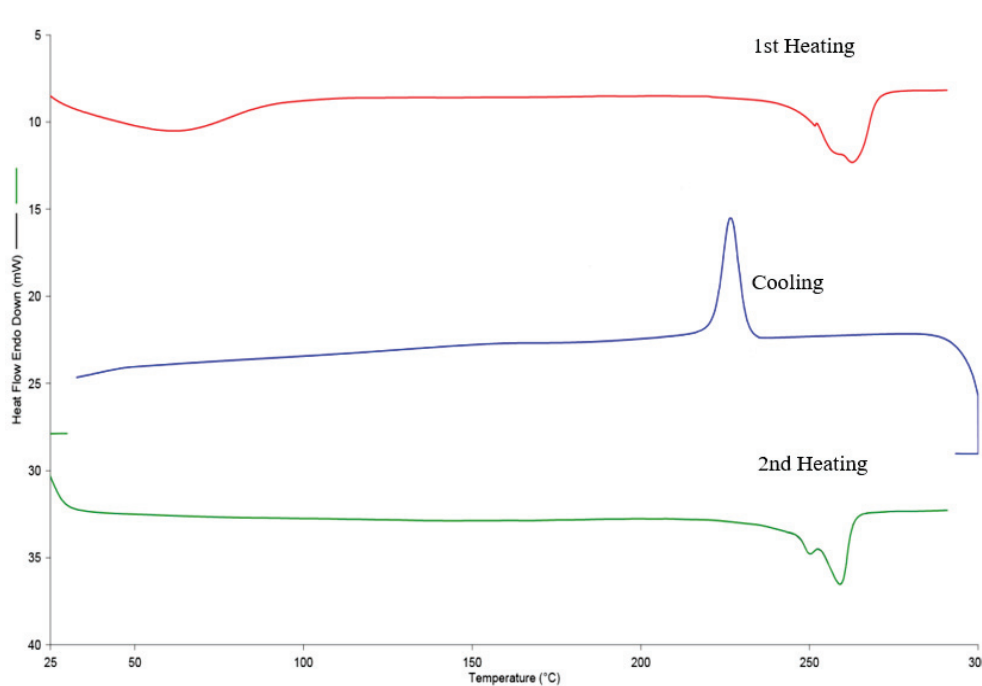


Figure 21. DSC graphs of 10% PA 66 + 0% rGO

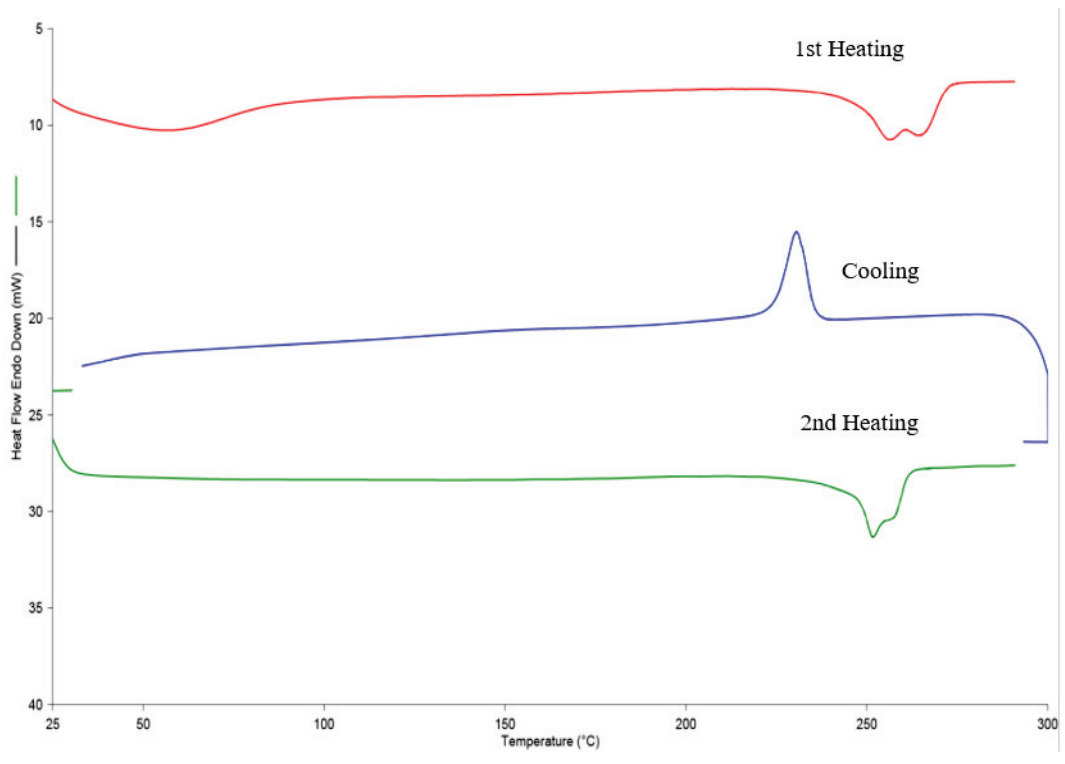


Figure 22. DSC graphs of 10% PA 66 + 1% rGO

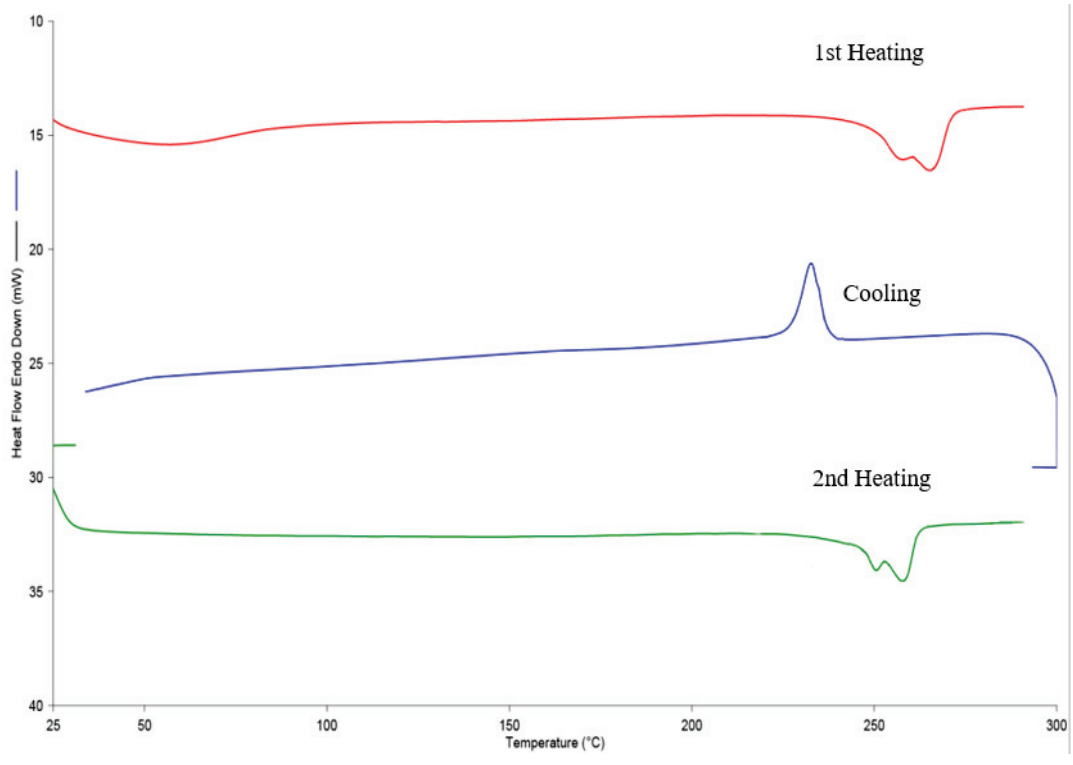


Figure 23. DSC graphs of 10% PA 66 + 2% rGO

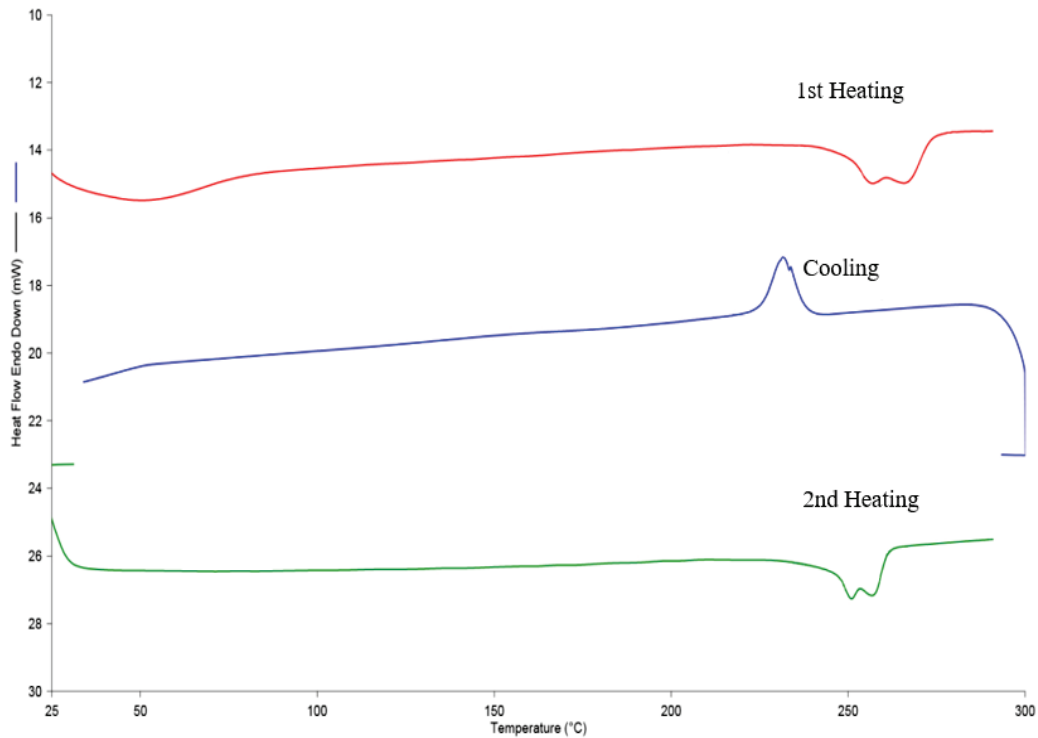


Figure 24. DSC graphs of 10% PA 66 + 3% rGO

### 4.3. Contact Angle Measurement Analysis

By means of contact angle measurement, the interaction of the adhesive with the surface can be determined. 3 samples were tested for each test group. Contact angle measurements of prepregs without nanofibers are given in Figure 25. The average contact angle measurement of three samples in the 60th second is 73.40°.

In Figure 26, contact angle measurements of prepregs coated with 10% PA 66 nanofibers are given. The average contact angle measurement of 3 samples in the 60th second is 35.13°. In Figure 27, contact angle measurements of prepregs coated with 10% PA 66+ 1%rGO nanofibers are given. The average contact angle measurement of 3 samples in the 60th second is 33.60°. In Figure 28, contact angle measurements of prepregs coated with 10% PA 66+ 2%rGO nanofibers are given. The average contact angle measurement of 3 samples in the 60th second is 26.18°. In Figure 29, contact angle measurements of prepregs coated with 10% PA 66+ 3%rGO nanofibers are given. The average contact angle measurement of 3 samples in the 60th second is 31.70°.

Contact angle measurements of prepregs and prepregs coated with nanofibers are given in Table 2. While the contact angle of prepregs not coated with nanofibers is high, the contact angle of 10% PA 66 nanofibers with 2% rGO added is the lowest.

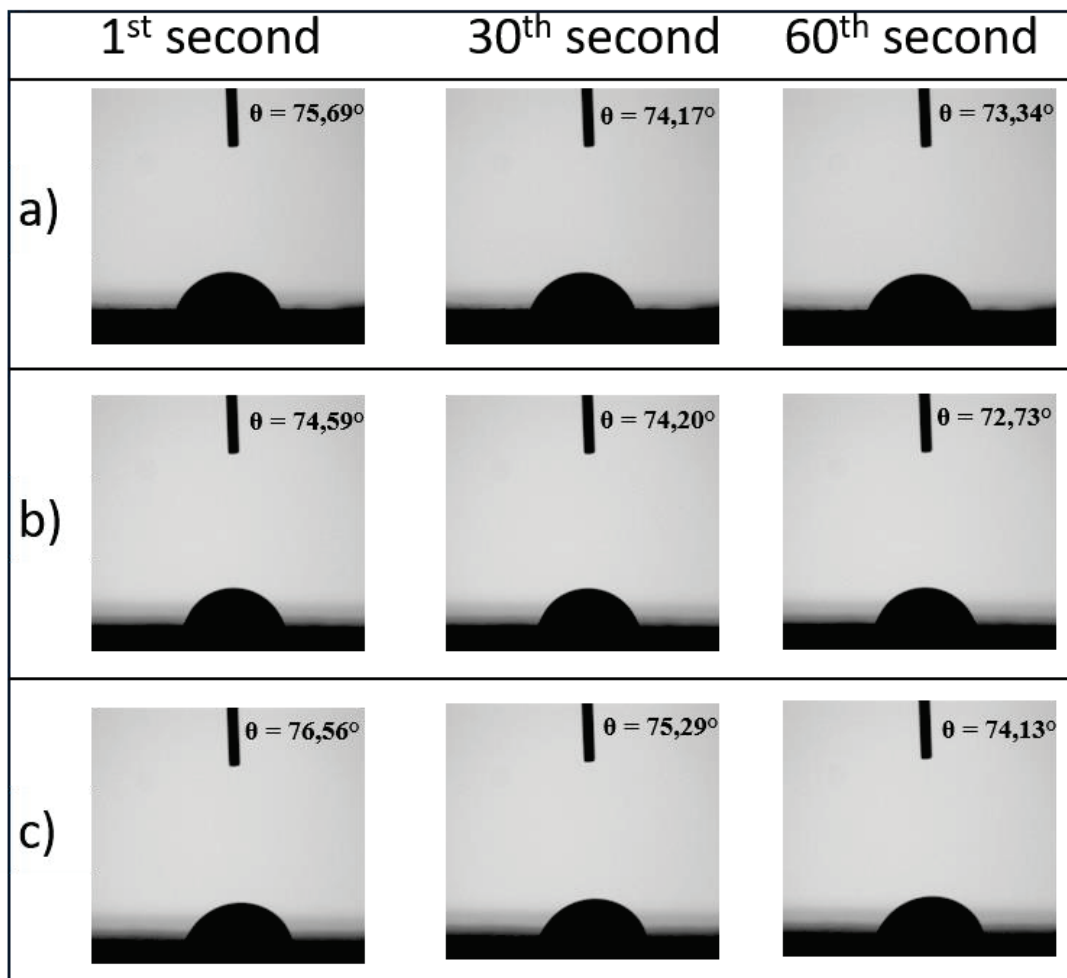


Figure 25. Images of the contact angle test measurements of the prepreg (without nanofibers) at 1st, 30th, and 60th seconds a)1<sup>st</sup> sample b)2<sup>nd</sup> sample c)3<sup>rd</sup> sample

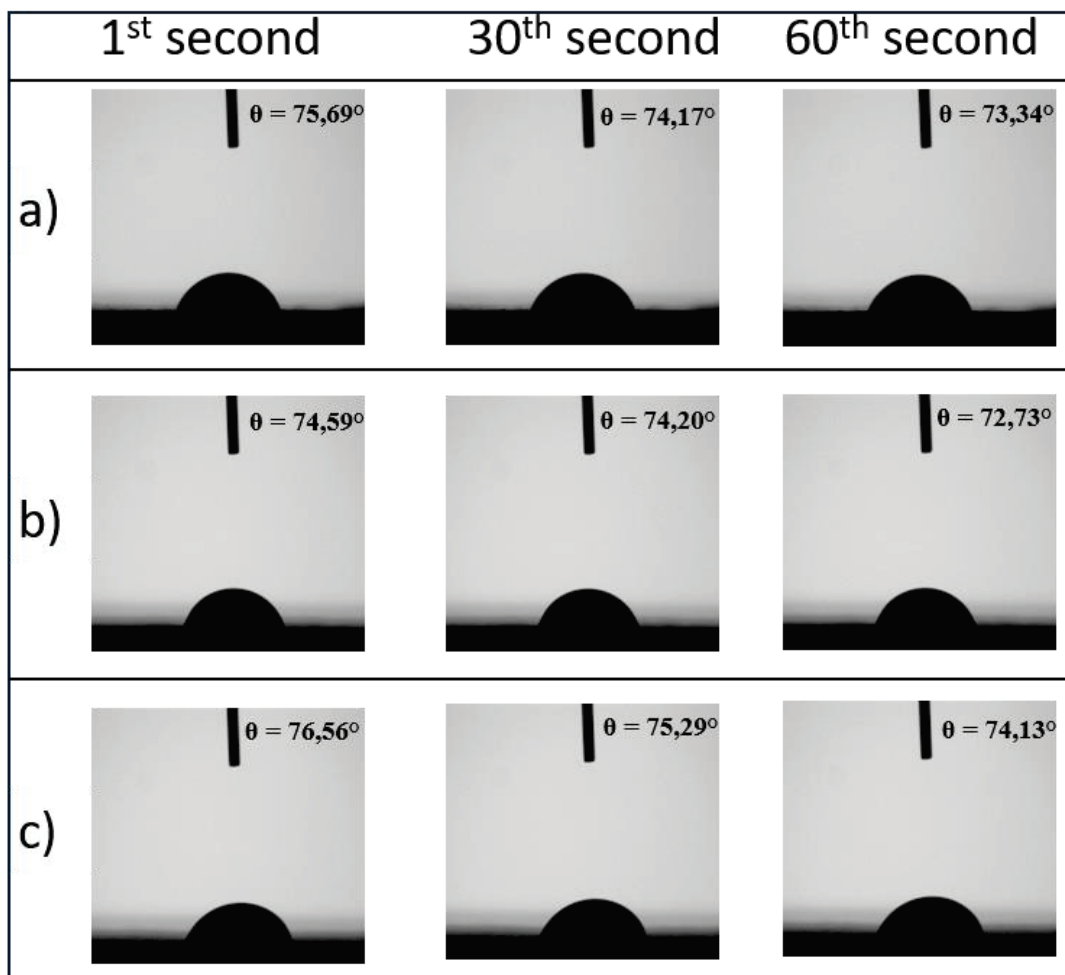


Figure 26. Images of contact angle test measurements of nanofibers containing 10% PA 66 + 0% rGO at 1st, 30th, and 60th seconds a)1<sup>st</sup> sample b)2<sup>nd</sup> sample c)3<sup>rd</sup> sample

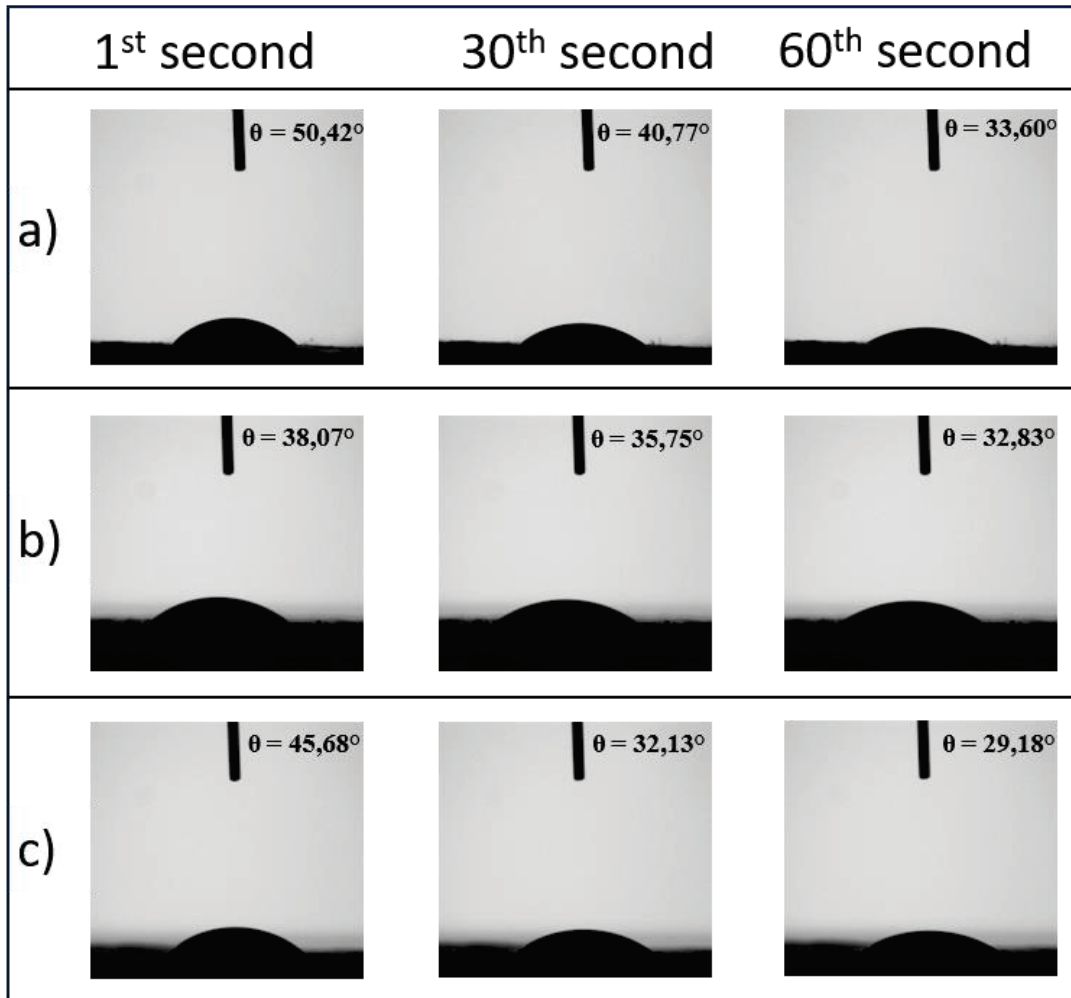


Figure 27. Images of contact angle test measurements of nanofibers containing 10% PA 66+ 1% rGO at 1st, 30th, and 60th seconds a)1<sup>st</sup> sample b)2<sup>nd</sup> sample c)3<sup>rd</sup> sample

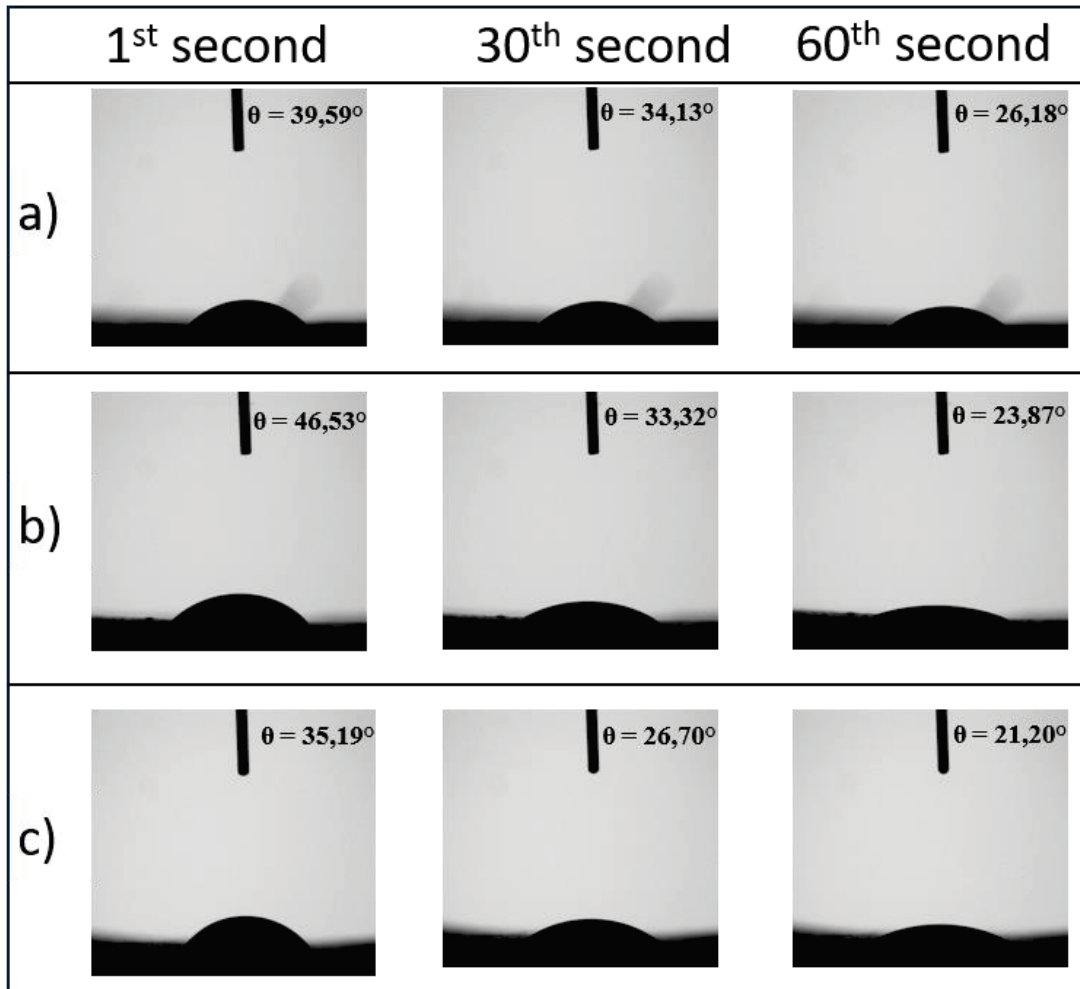


Figure 28. Images of contact angle test measurements of nanofibers containing 10% PA 66 + 2% rGO at 1st, 30th, and 60th seconds a)1<sup>st</sup> sample b)2<sup>nd</sup> sample c)3<sup>rd</sup> Sample

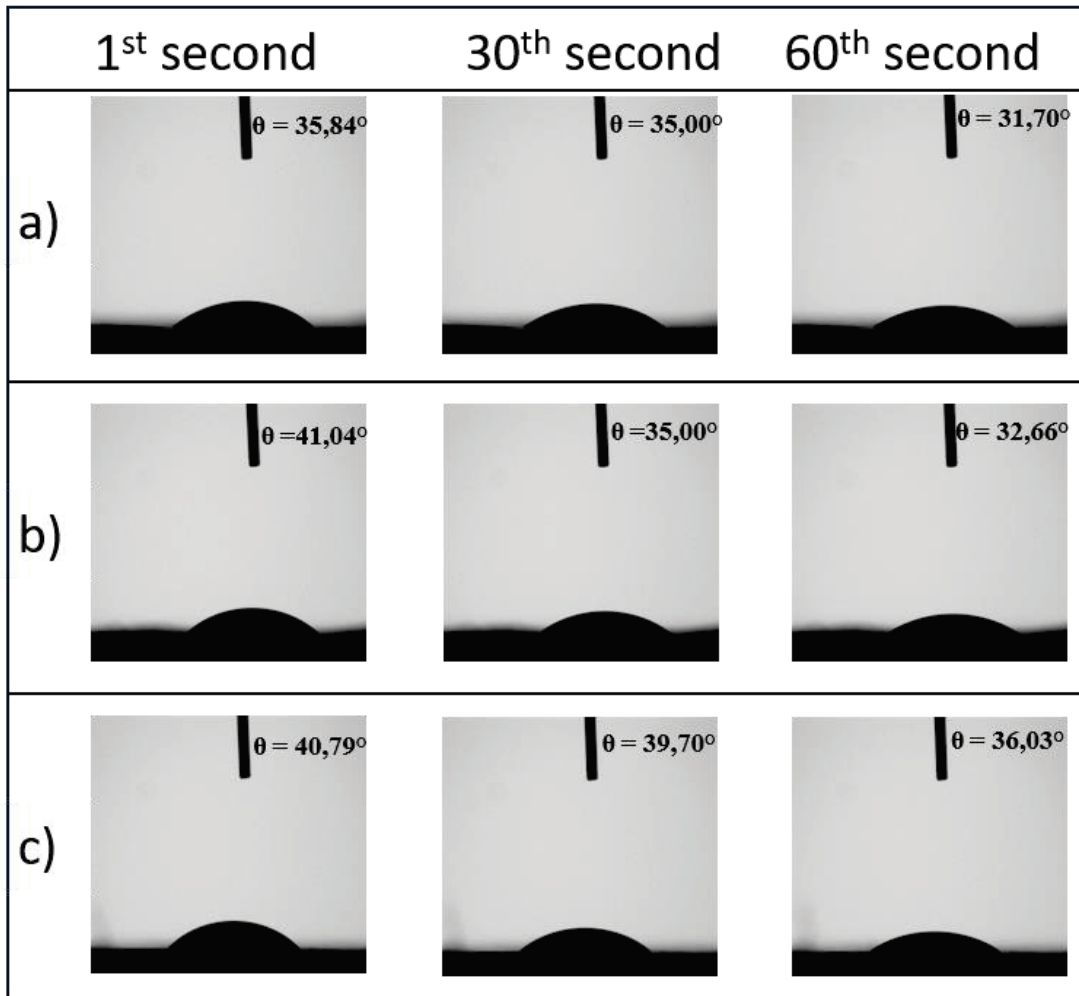


Figure 29. Images of contact angle test measurements of nanofibers containing 10% PA 66+ 3% rGO at 1st, 30th, and 60th seconds a)1<sup>st</sup> sample b)2<sup>nd</sup> sample c)3<sup>rd</sup> sample

Table 2. Contact angle measurements of prepregs and PA 66 and PA66/rGO nanofiber coated prepregs

Samples	$\theta$ (°)	Average $\theta$ (°)
%0 PA 66 + %0 rGO_1	73.34	73.40±0.57
%0 PA 66 + %0 rGO_2	72.73	
%0 PA 66 + %0 rGO_3	74.13	
%10 PA 66 + %0 rGO_1	36.34	35.13±2.17
%10 PA 66 + %0 rGO_2	36.98	
%10 PA 66 + %0 rGO_3	32.08	
%10 PA 66 + %1 rGO_1	33.60	33.60±1.93
%10 PA 66 + %1 rGO_2	32.83	
%10 PA 66 + %1 rGO_3	29.18	
%10 PA 66 + %2 rGO_1	26.18	26.18±2.03
%10 PA 66 + %2 rGO_2	23.87	
%10 PA 66 + %2 rGO_3	21.20	
%10 PA 66 + %3 rGO_1	31.70	31.70±1.86
%10 PA 66 + %3 rGO_2	32.66	
%10 PA 66 + %3 rGO_3	36.03	

#### 4.4. Single Lap Joints (SLJ) Test

The composite plates were joined in a hot press using 3 FM 300K film adhesive plies. Test coupons are prepared according to ASTM D5868 standard. Figure 30. shows an image of a Single Lap Joints Test sample during testing.



Figure 30. Image of a single lap joints test sample

The load-displacement diagrams of composite plates of the Single Lap Joints test are shown, respectively, 0% PA 66 + %0 rGO in Figure 31, 10% PA 66 + %0 rGO in Figure 32, 10% PA 66 + %1 rGO in Figure 33, 10% PA 66 + %2 rGO in Figure 34, and 10% PA 66 + %3 rGO in Figure 35. In Figure 36, the stress value calculated according to the load-displacement curve and considering the joint cross-sectional area is given in the bar graph. When the results are examined, it is clearly seen that rGO added up to 2% causes an increase in the strength of the joint area. The average stress value of test coupons without nanofibers is 14.14 MPa. The average stress value of the composite plate covered with 10% PA 66 nanofiber in the joint area was 16.18 MPa, and an increase of 14.43% was recorded in the strength. The mean stress values of 1% rGO and 2%rGO added nanofibers were 16.27 MPa and 16.67 MPa, respectively. There was a 15.06% improvement in test coupons with 1% rGO addition, and 17.89% improvement in test coupons with 2% rGO addition. The average stress value of test coupons with 3%rGO added is 15.55 MPa. The increase tended to decrease when 3% rGO was added, with a 9.97% increase reported compared to samples without nanofibers. Therefore, the addition of 2% rGO was determined as the optimum value. Table 3 shows the average stress results of the Lap shear test.

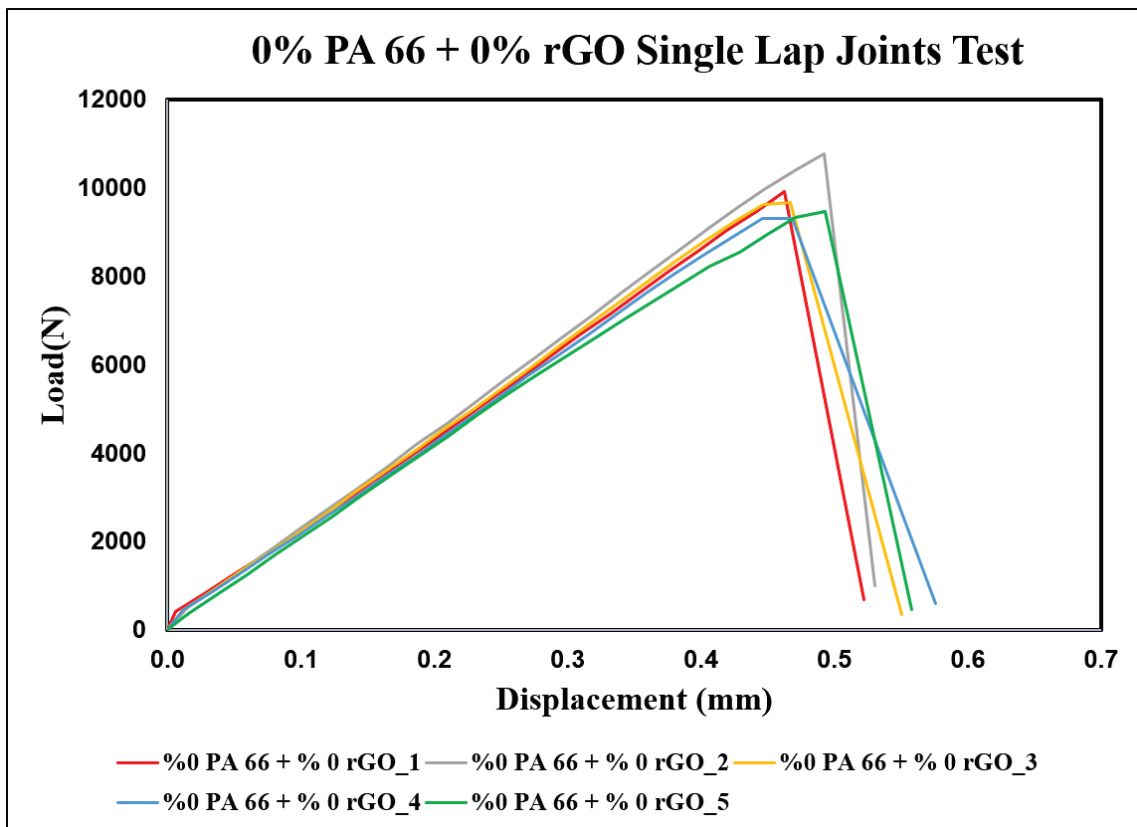


Figure 31. The load-displacement curve of 0% PA 66 + 0% rGO (without nanofibers) composite plates

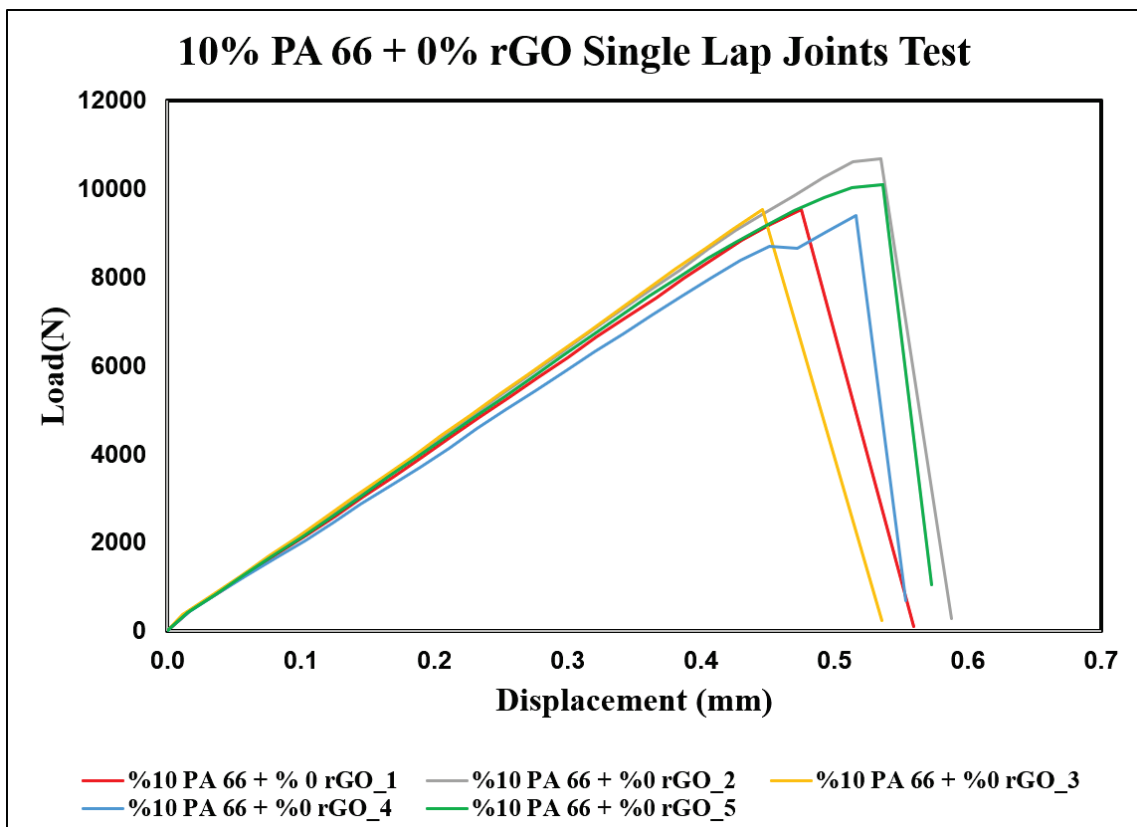


Figure 32. The load-displacement curve of 10% PA 66 + 0% rGO composite plates

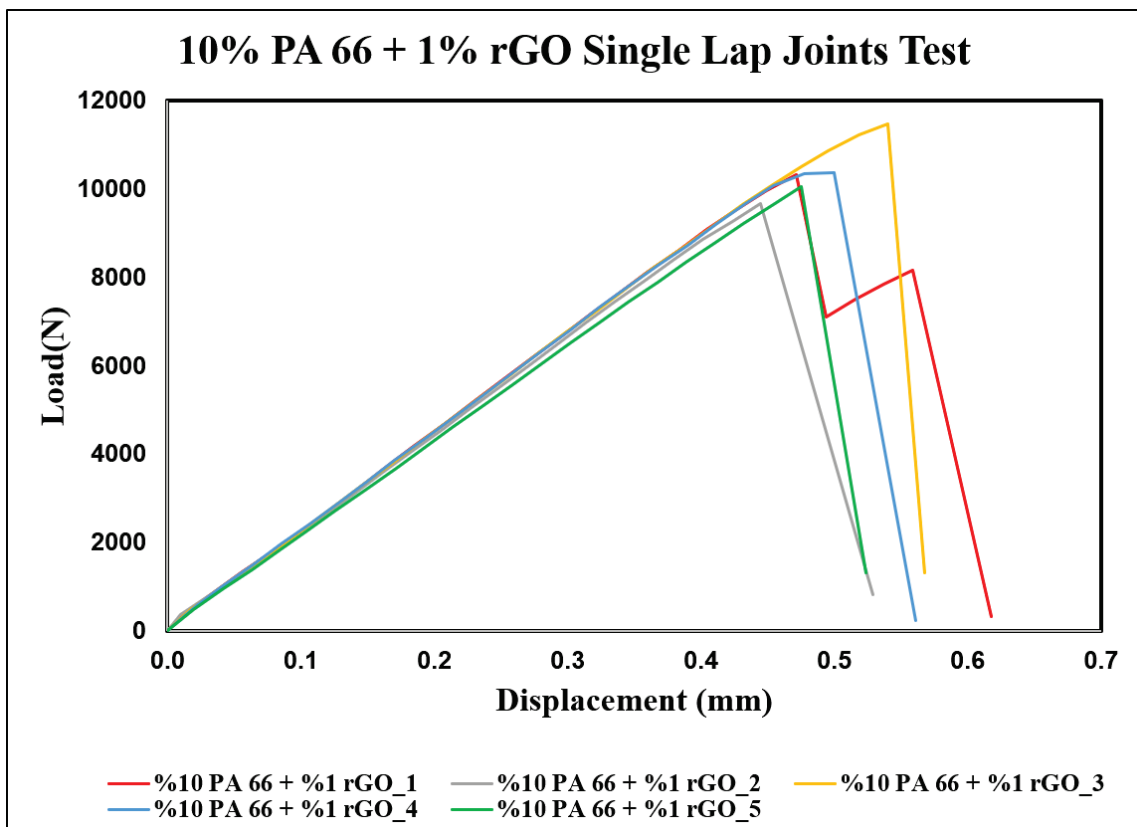


Figure 33. The load-displacement curve of 10% PA 66 + 1% rGO composite plates

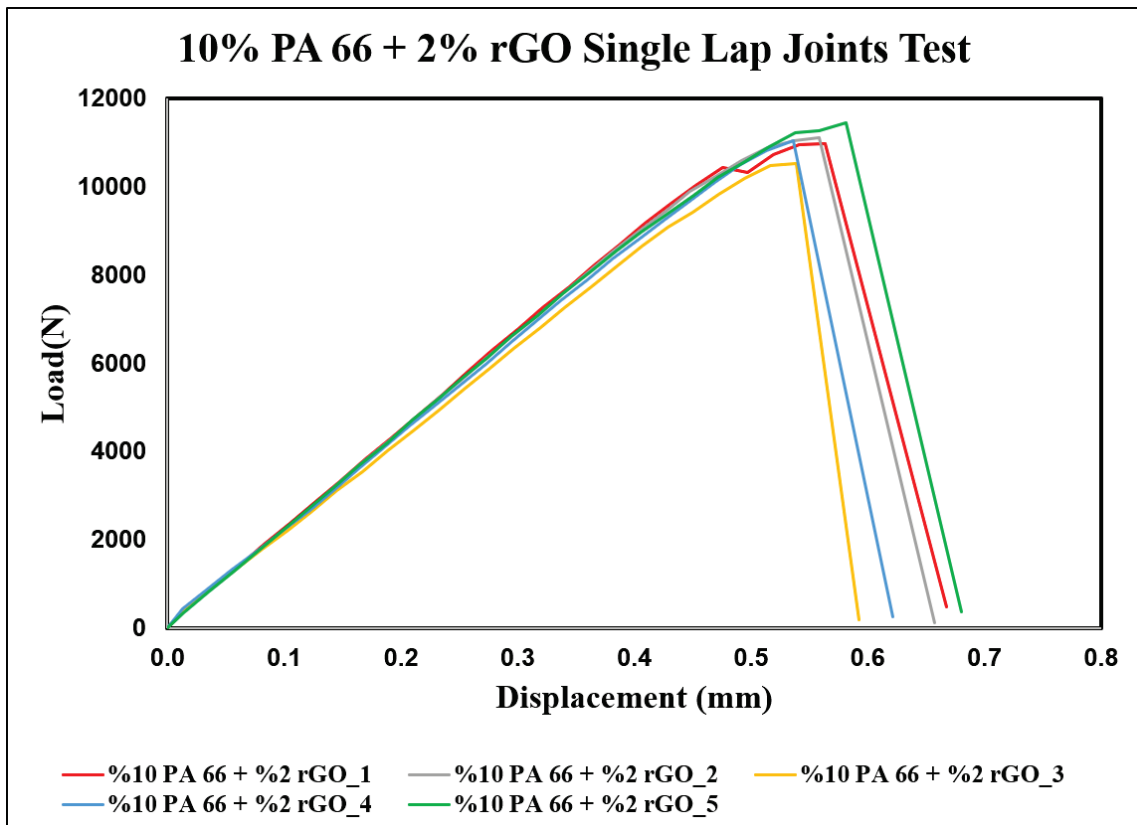


Figure 34. The load-displacement curve of 10% PA 66 + 2% rGO composite plates

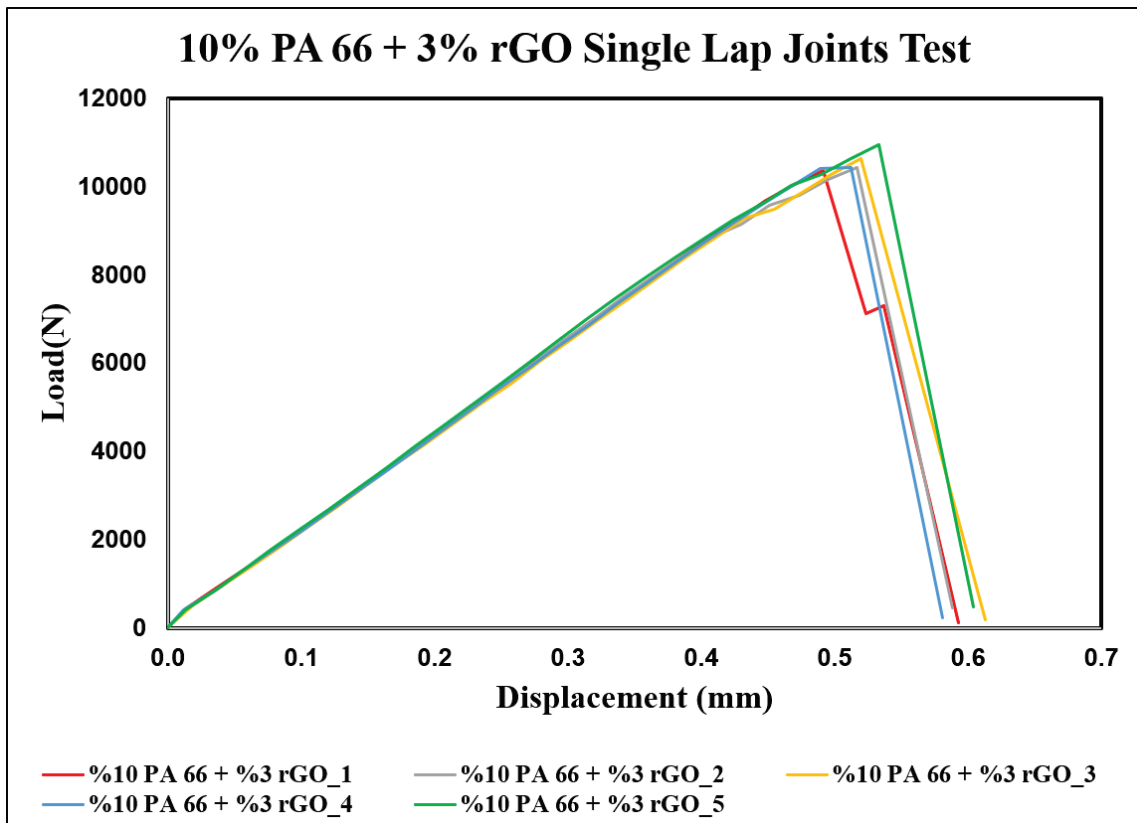


Figure 35. The load-displacement curve of 10% PA 66 + 3% rGO composite plates

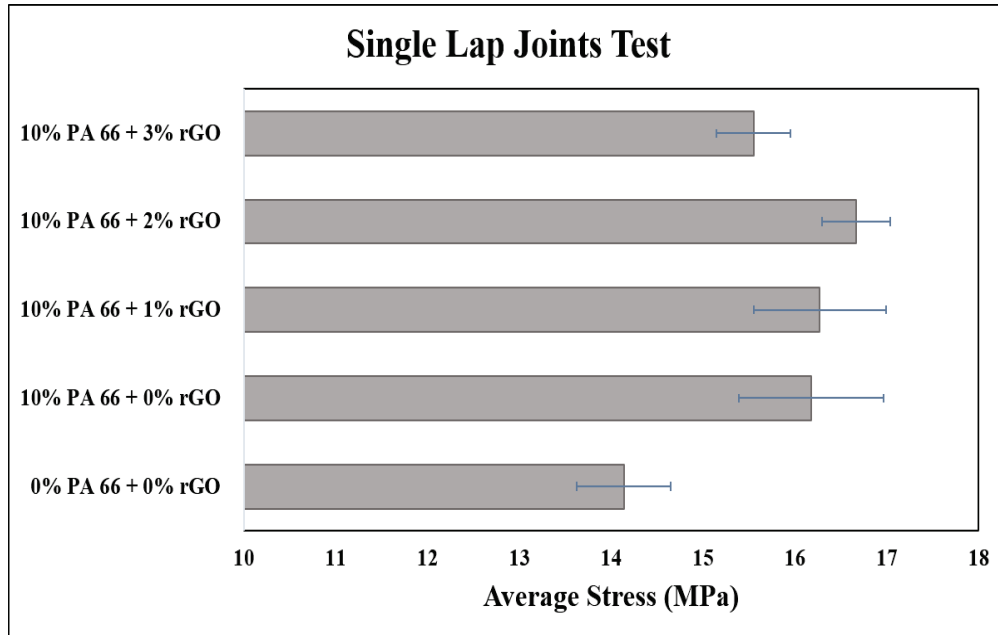


Figure 36. Average stress values of single lap joints test results

Table 3. The average stress results of the single lap joints test.

	<b>Average Stress (MPa)</b>	<b>Standard Deviation</b>	<b>% Increase</b>
%0 PA 66 + %0 rGO	14.14	±0.51	
%10 PA 66 + %0 rGO	16.18	±0.79	14.43%
%10 PA 66 + %1 rGO	16.27	±0.72	15.06%
%10 PA 66 + %2 rGO	16.67	±0.37	17.89%
%10 PA 66 + %3 rGO	15.55	±0.40	9.97%

The fracture behavior of the sample also gives important information about the adhesion of the adhesive to the joint surface. Fracture surfaces of the single lap joints test specimens are shown in Figure 37. All samples showed mixed fracture behavior (adhesive failure – fiber tear failure). However, while the adhesive failure density is high in the samples that are not modified with nanofiber, the fiber tear failure mode increases with the increase of nanofiber modified and graphene addition. SEM images of the fracture surface of the Single lap joints test coupons are given in Figure 38. SEM images also support the failure mode observed on the fracture surface. It is seen that the adhesive adheres less to the sample surface that is not modified with nanofibers.

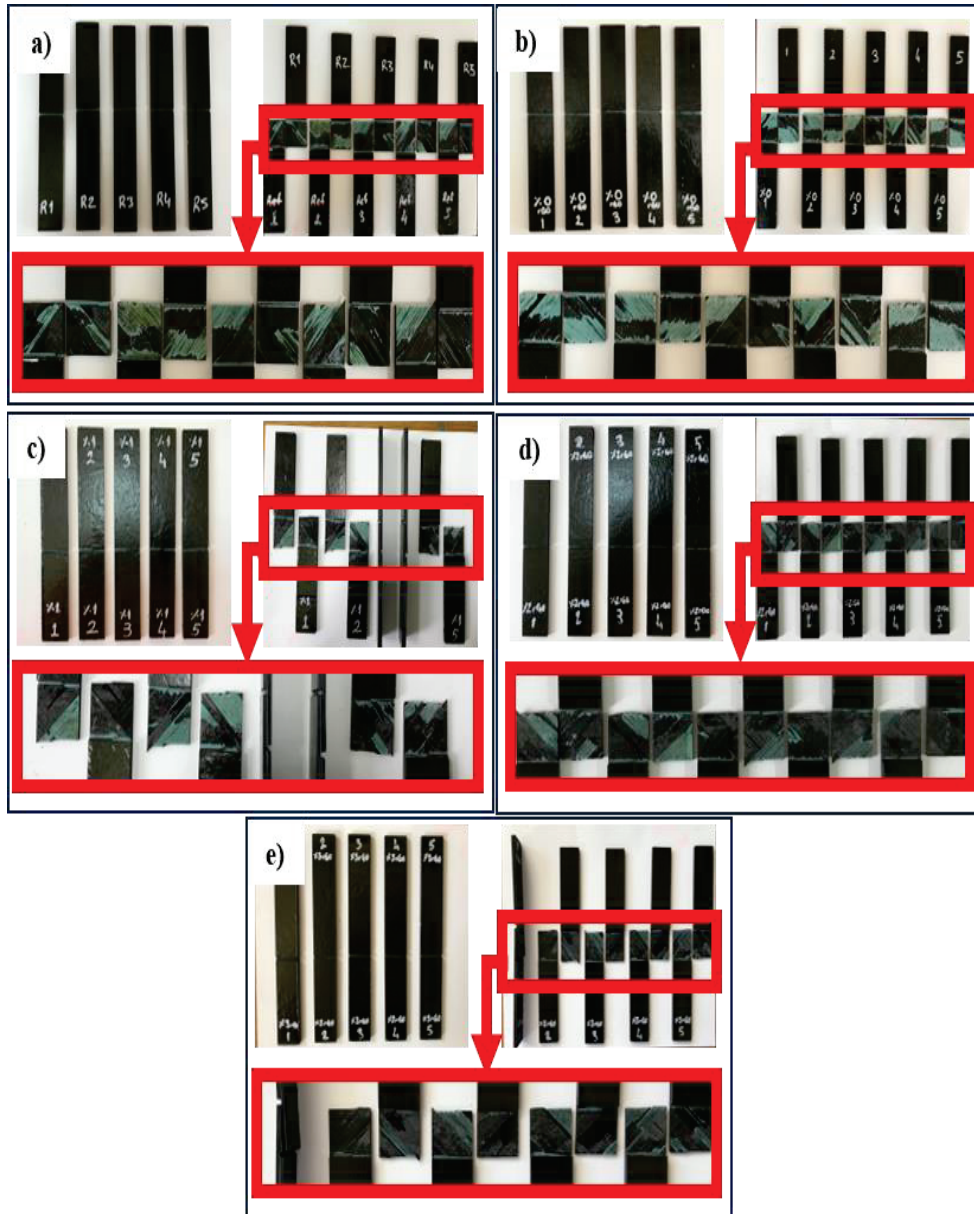


Figure 37. Before and after test images of single lap joints test specimens a) 0% PA 66 + 0% rGO (without nanofibers), b) 10% PA 66 + 0% rGO, c) 10% PA 66 + 1% rGO, d) 10% PA 66 + 2% rGO and, e) 10% PA 66 + 3% rGO.

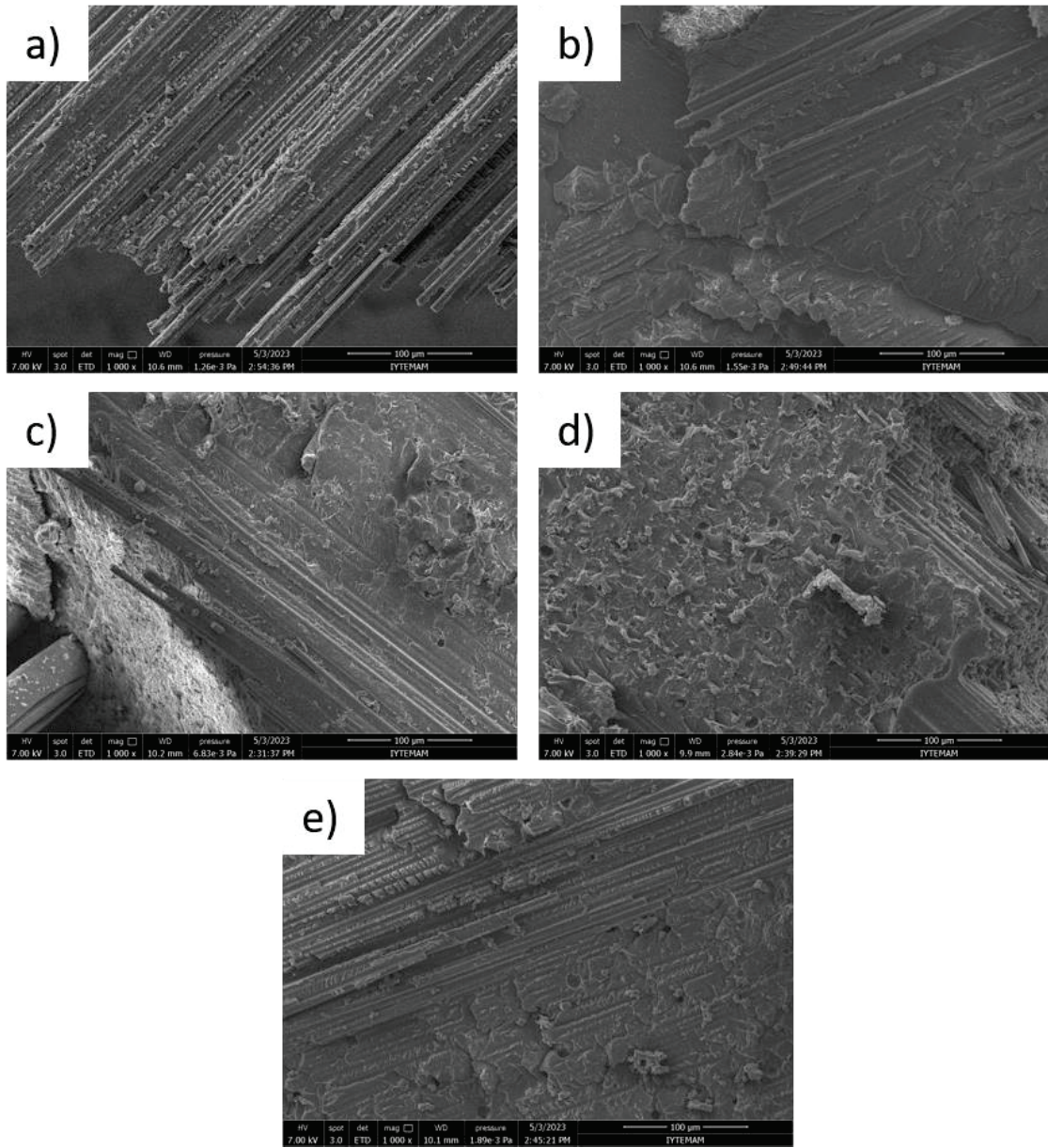


Figure 38. Fracture surface images of single lap joints test specimens a) 0% PA 66 + 0% rGO (without nanofibers), b) 10% PA 66 + 0% rGO, c) 10% PA 66 + 1% rGO, d) 10% PA 66 + 2% rGO and, e) 10% PA 66 + 3% rGO.

## 4.5. Charpy Impact Test

Modified and unmodified carbon epoxy plates with and without rGO nanofibers were bonded with 3 plies of FM 300 K film adhesive. The Charpy impact test was performed to determine the impact strength of the joining parts. Coupons are prepared according to ISO 179-1 standard. Figure 39. shows the test moment image of the V-notch Charpy impact test coupon.

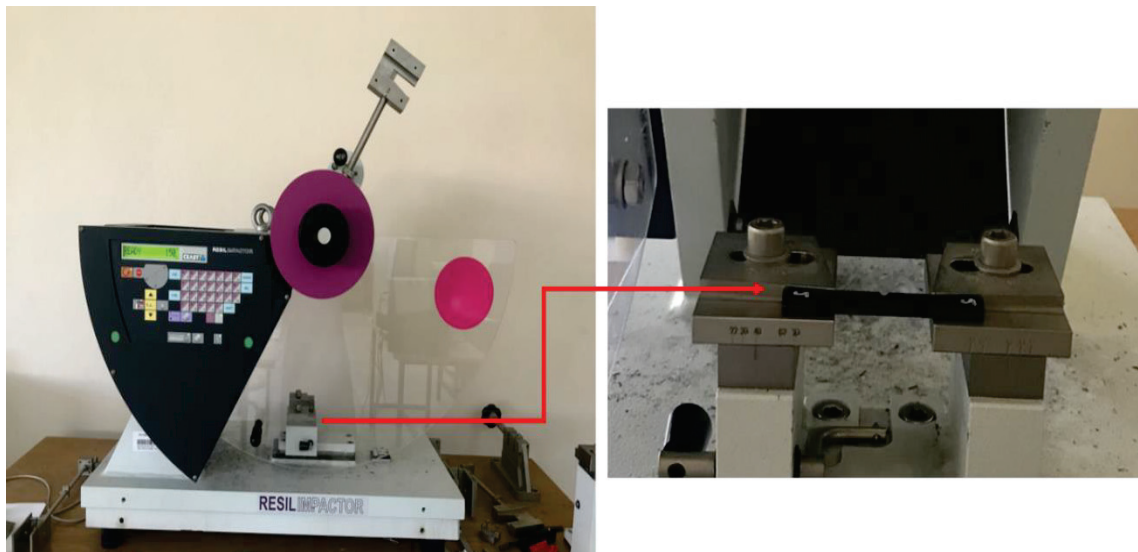


Figure 39. Image of the Charpy impact test sample

Charpy impact strength results of samples undergoing Charpy impact test are shown in Table 4. According to the results in the table, the average results of the Charpy impact strength are given in the form of a bar graph in Figure 40. When the results were examined, the impact strengths of the unmodified, 10% PA 66 nanofibers and modified with 1% rGO, 2% rGO and 3%rGO added to the nanofibers were 111.23, 129.98, 141.97, 145.25 and 118.08 kJ/m<sup>2</sup>, respectively. While an improvement of 16.86% was observed in the plates modified with 10% PA 66 nanofibers, the impact strength of the plates modified with nanofibers by adding 1%rGO, 2% rGO and 3%rGO was reported to improve by 27.64%, 30.59% and 6.16%, respectively. When 3% rGO is added, a decrease in the increase in impact strength is observed. These results, which are also consistent with the single lap joints test, show that the addition of 3% rGO exceeds the saturation point of the solution. As a result, the addition of 2% rGO was determined as the optimum value in the Charpy impact strength results. It is clearly seen that the addition of PA 66 nanofibers and graphene increases the impact strength by causing impact absorption

Table 4. The Charpy impact test results.

Samples Number	0% PA66 +0% rGO (kJ/m <sup>2</sup> )	10% PA66 +0% rGO (kJ/m <sup>2</sup> )	10% PA66 +1% rGO (kJ/m <sup>2</sup> )	10% PA66 +2% rGO (kJ/m <sup>2</sup> )	10% PA66 +3% rGO (kJ/m <sup>2</sup> )
1	120.25	151.16	132.64	163.42	127.96
2	104.01	119.47	131.46	153.92	116.57
3	100.52	155.84	152.30	162.15	123.14
4	101.17	140.64	157.87	131.02	132.29
5	118.76	125.80	144.44	122.95	118.74
6	121.29	115.95	148.93	148.78	104.49
7	112.79	113.10	138.37	156.02	112.43
8	122.25	113.06	148.06	140.81	115.95
9	100.57	125.29	125.52	127.26	113.18
10	110.68	139.54	140.12	146.17	116.10
Average	<b>111.23</b>	<b>129.98</b>	<b>141.97</b>	<b>145.25</b>	<b>118.08</b>
Standard Dev.	<b>±8.63</b>	<b>±14.97</b>	<b>±9.67</b>	<b>±13.65</b>	<b>±7.60</b>
%Increase		<b>16.86%</b>	<b>27.64%</b>	<b>30.59%</b>	<b>6.16%</b>

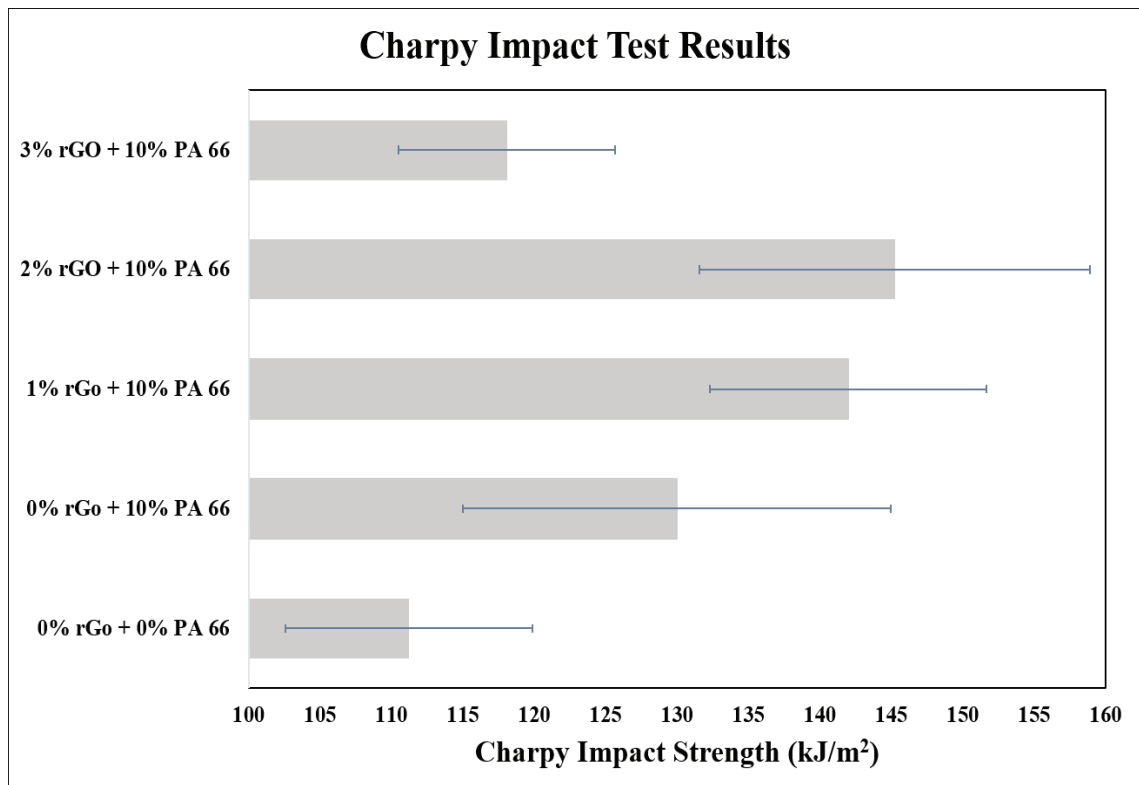


Figure 40. Average stress values of Charpy impact test results

Figure 41 shows before and after test images of Charpy impact test coupons. After the test, the morphological structure of the fracture zone was analyzed by SEM. SEM images of the fracture region of the Charpy impact test coupons are given in Figure 42. When the structure of the broken fibers in the unmodified test coupons is examined, it is seen that there is less adhesive on it compared to the modified coupons and the breakage is more regular. In the modified coupons, it is seen that the breakage is more irregular and the adhesive adheres to the fibers more. It is supported by the refractive images of the fibers in which PA 66 nanofibers and rGO contribute to the impact energy absorption.

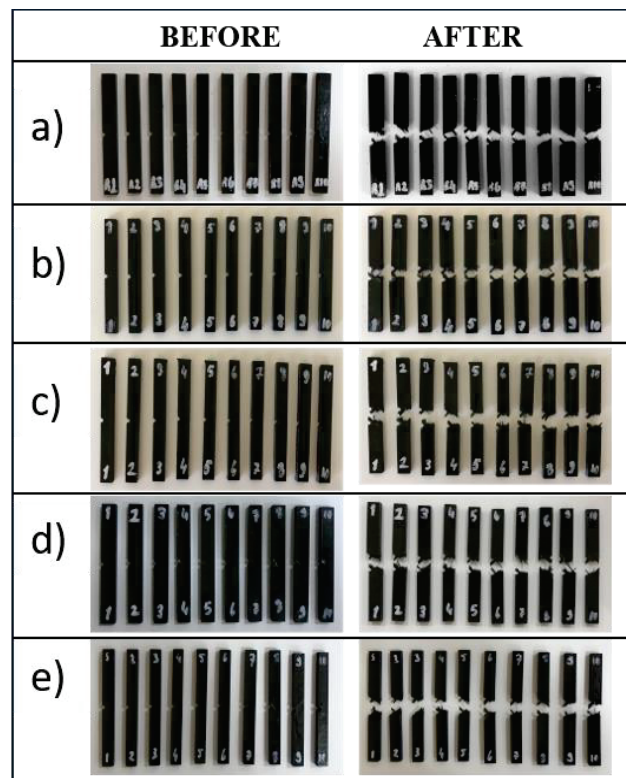


Figure 41. Before and after test images of Charpy impact test specimens a) 0% PA 66 + %0 rGO (without nanofibers), b) 10% PA 66 + %0 rGO, c) 10% PA 66 + %1 rGO, d) 10% PA 66 + %2, rGO and, e) 10% PA 66 + %3 rGO.

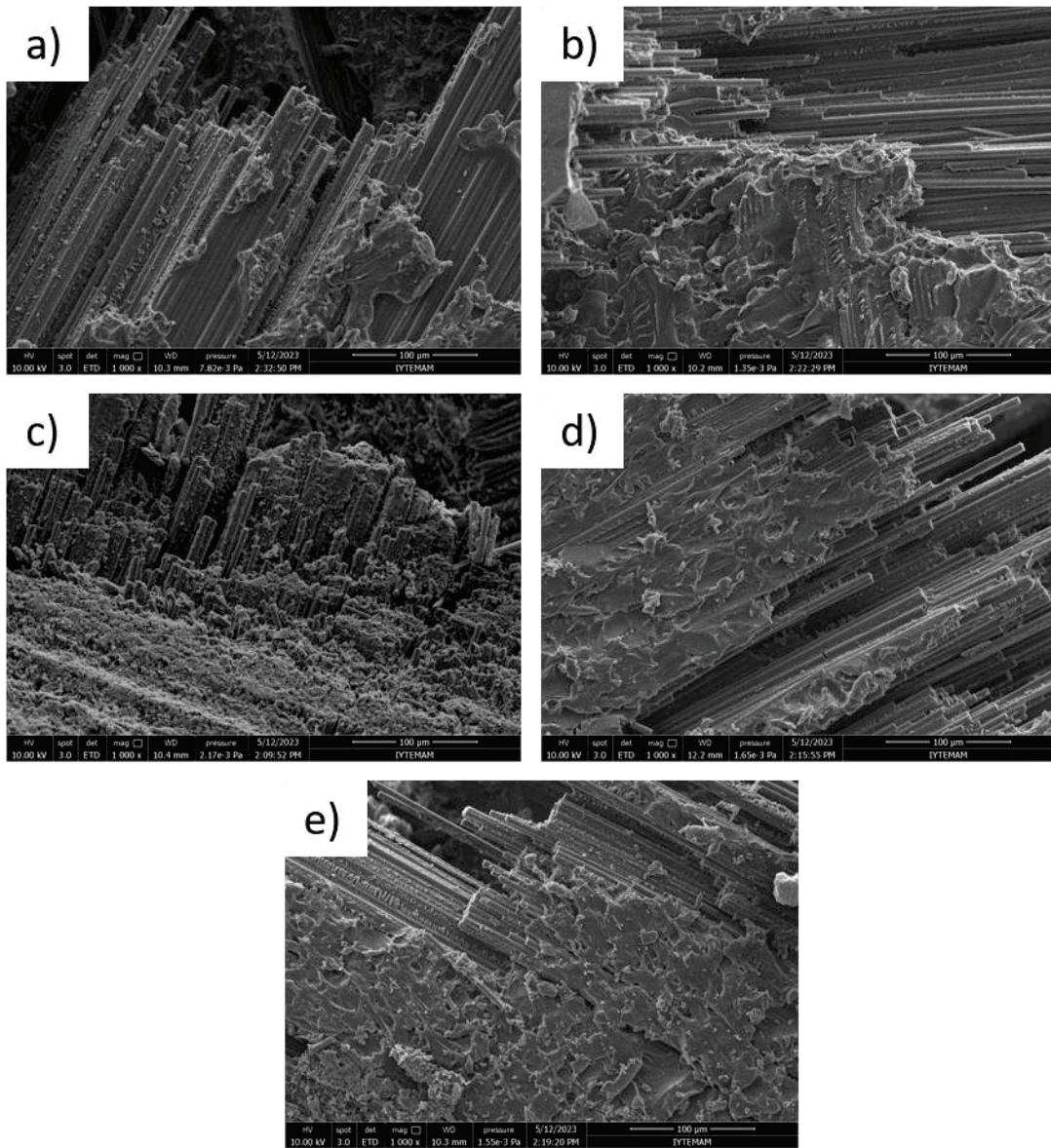


Figure 42. Fracture surface images of Charpy impact test specimens a) 0% PA 66 + %0 rGO (without nanofibers), b) 10% PA 66 + %0 rGO, c) 10% PA 66 + %1 rGO, d) 10% PA 66 + %2, rGO and, e) 10% PA 66 + %3 rGO.

## CHAPTER 5

### CONCLUSION

Due to its advantages, composite materials are preferred, especially in the aviation industry. These materials, which provide high strength, do not cause negative effects such as serious increases in weight and corrosion. With this advantage of composite materials, the joining of composites has also become an important issue. Conventional joining methods used cause severe delamination, weight gain, and stress accumulation in the joint area in fiber-reinforced composites. Therefore, combining composites with innovative methods such as film adhesive is an important research topic. Combining with the film adhesive does not cause a serious increase in weight, causing corrosion, and the load is distributed uniformly, not in a single region. However, in order for the adhesive to adhere well to the surface, it must form a strong bond with the composite surface. Therefore, surface modification is necessary.

In this study, carbon/epoxy prepreg was coated with PA 66 nanofibers and rGO added PA 66 nanofibers. A solution containing 10% wt/v of PA 66 was obtained by dissolving 10 g of PA 66 pellets in 100 ml of formic acid and chloroform (75:25 v/v). In addition, rGO was added to the solution at 1%, 2% and 3% wt/v ratios. Using the obtained solution, the prepreg fabrics were coated with electrospun rGO added nanofibers. The coated prepregs have a fiber orientation of 45° and are located in the junction area (top layer). After the carbon prepregs are laid cleanly, they are turned into plates in the hot press. Thus, composite plates modified with nanofibers on the surface and rGO to further strengthen the mechanical performance are obtained. The surface is then cleaned with ethyl alcohol with a gentle buffering action. It is joined in the hot press by the secondary bonding method using 3 plies of FM 300 K film adhesive.

SEM analyses to determine the morphological properties of nanofibers, DSC analyses to examine thermal properties, and contact angle tests to examine contact angle were performed. SLJ and Charpy impact tests were performed to examine the mechanical properties.

Nanofiber structure and dispersion of graphene were investigated by SEM analysis. The nanofibers formed with 10% wt/v ratio of PA 66 pellets have an average diameter of 44.08 nm. When the morphological structure of nanofibers is examined, a

beadless nanofiber structure is observed. 1%, 2%, and 3% wt/v ratios of rGO were added to the solution prepared at 10% PA 66 wt/v ratio. It was revealed by SEM that the rGO was approximately 5  $\mu\text{m}$  wide. SEM images show that graphene is spread over all regions of the nanofiber network. It has been determined that the rGO layers added at the rate of 3% wt/v are not in a monolayer structure by overlapping.

The nanofibers were cured in the hot press at 135°C for 2 hours and then at 180°C for 2 hours under 7 bar pressure together with the prepregs. In order to examine the effect of temperature and pressure, the aluminum foil and the prepreg were coated with PA 66 nanofibers and then pressed in the hot press at the specified temperature and pressure conditions. When the structure of nanofibers pressed by coating on aluminum foil was examined by SEM, it was determined that the mobility of nanofibers decreased by bonding with each other. When the morphological structure of the nanofibers pressed by coating on the prepreg was examined, it was determined that the nanofibers were embedded in the prepreg by bonding with epoxy.

Thermal properties of PA 66 nanofibers at 10% wt/v ratio and nanofibers formed with 1%, 2%, and 3% wt/v ratio rGO added to PA 66 nanofibers were investigated by DSC. All samples were analyzed as first heating, cooling and reheating. While the addition of rGO had no effect on the melting temperature, it was found that it slightly accelerated the crystallization when the cooling curve was examined.

Contact angle test was performed to examine whether the junction surface is hydrophilic and hydrophobic. The low contact angle is due to the hydrophilic nature of the surface. It is expected that the hydrophilic surface will establish a better bond with the adhesive and the adhesive will adhere more strongly to the surface. The average contact angle of the prepreg surface not modified with nanofibers is 73.40°. The mean contact angle measurements of the nanofibers with 10% PA 66 nanofibers and additional 1%, 2%, and 3% wt/v rGO added to the nanofibers on the prepreg are 35.13°, 33.60°, 26.18°, and 31.70°, respectively. It was determined that the most hydrophilic surface was the prepreg surface coated with 2% wt/v rGO added PA 66 nanofibers.

SLJ tests were carried out to examine the joint characteristics of the joined composite parts and to determine the bond strength. According to the results of the SLJ tests, it is seen that there is an increase of 14.43 % against the unmodified surface in the composite parts with 10% wt/v PA 66 nanofibers modified. In addition, an increase of 15.06%, 17.89%, and 9.97% is observed in PA 66 nanofibers with 1%, 2% and 3% rGO added, respectively. When the fracture surface of the samples is examined after the test,

mixed failure (fiber tear failure) is observed. However, it is seen that the fiber tear failure mode increases on the modified surfaces.

In order to examine the impact behavior of nanofiber modified and unmodified composite parts, the Charpy impact strength was investigated with the Charpy Impact test. The surface modified with 10% wt/v ratio of PA 66 nanofibers showed an increase of 16.86% compared to the unmodified surface. In addition, an increase of 27.64%, 30.59%, and 6.16% was observed in PA 66 nanofibers with 1%, 2% and 3% rGO added versus unmodified surface.

Parameters such as the materials in the electrospinning solution (formic acid, chloroform, and PA 66 pellets) used in this study, the nano-filling material (rGO) added to the solution, the fabric used (carbon/epoxy prepreg), the secondary bonding method, the composite production in a hot press affect the output. New studies can be made with different solutions, different nano-filling additions (such as CNT) and different bonding techniques (co-curing, co-bonding) and different production techniques (such as hand lay-up, autoclave oven). Hybrid bonding can be done by using mechanical fastening together with the adhesive in production. Tests such as End-Notched-Flexure (ENF) test, The asymmetric double cantilever beam (ADCB), The calibrated-end-loaded split (C-ELS) test of composite parts modified with PA 66 and PA 66/rGO nanofibers can be applied.

## REFERENCES

- [1] "Composite." Oxford Learner's Dictionaries. Accessed June 13, 2023. [https://www.oxfordlearnersdictionaries.com/definition/english/composite\\_2](https://www.oxfordlearnersdictionaries.com/definition/english/composite_2).
- [2] Callister, William D. 1991. *Materials Science and Engineering: An Introduction*. 2nd ed. [https://doi.org/10.1016/0261-3069\(91\)90101-9](https://doi.org/10.1016/0261-3069(91)90101-9).
- [3] Nagavally, Rahul Reddy. "Composite Materials -History, Types, Fabrication Techniques, Advantages, and Applications." Conference, India, July 24, 2016.
- [4] Beylergil, Bertan. "Toughening of Carbon Fiber Based Composites with Electrospun Fabric Layers." Doctoral dissertation, Izmir Institute of Technology, 2017.
- [5] "History of Composites." Discover Composites. Accessed June 14, 2023. <https://discovercomposites.com/what-are-composites/history-of-composites/>.
- [6] Harris, Bryan. 1999. *Engineering Composite Materials*. London.
- [7] Shehab, Essam, Arshyn Meiirbekov, Akniyet Amantayeva, and Serik Tokbolat. "Cost Modelling for Recycling Fiber-Reinforced Composites: State-of-the-Art and Future Research." *Polymers* 15, no. 1 (2023). <https://doi.org/10.3390/polym15010150>.
- [8] D. K. Rajak, P. H. Wagh, and E. Linul, "Manufacturing Technologies of Carbon/Glass Fiber-Reinforced Polymer Composites and Their Properties: A review," *Polymers*, vol. 13, no. 21. MDPI, Nov. 01, 2021. doi: 10.3390/polym13213721.
- [9] A. McIlhagger, E. Archer, and R. McIlhagger, "Manufacturing Processes for Composite Materials and Components for Aerospace Applications," in *Polymer Composites in the Aerospace Industry*, Elsevier, 2019, pp. 59–81. doi: 10.1016/B978-0-08-102679-3.00003-4.
- [10] J. Mohan, A. Ivanković, and N. Murphy, "Mixed-mode fracture toughness of co-cured and secondary bonded composite joints," *Engineering Fracture Mechanics*, vol. 134, pp. 148–167, 2015, doi: 10.1016/j.engfracmech.2014.12.005.
- [11] X. Wu, K. He, Z. Gong, Z. Liu, and J. Jiang, "The Shear Strength of Composite Secondary Bonded Single-Lap Joints with Different Fabrication Methods," *Journal of Adhesion Science and Technology*, vol. 34, no. 9, pp. 936–948, May 2020, doi: 10.1080/01694243.2019.1690775.
- [12] Paranjpe and Nikhil, "Strength And Failure Mode Analysis Of Composite-to-Composite and Composite-to-Metal Single Lap Joints with Different Surface Treatments," Master's Thesis, Wichita State University, 2016.

- [13] K. S. Kim, J. S. Yoo, Y. M. Yi, and C. G. Kim, "Failure Mode and Strength of Uni-directional Composite Single Lap Bonded Joints with Different Bonding Methods," *Composite Structures*, vol. 72, no. 4, pp. 477–485, Apr. 2006, doi: 10.1016/j.compstruct.2005.01.023.
- [14] A. Sadeghi, R. Mahshid, M. Heidari-Rarani, and L. Lessard, "Effect of Lamina Fiber Orientation Interfaced with Semi-Flexible Adhesive Layer on Strength and Failure Mode of Composite Single-Lap Joints," *International Journal of Adhesion and Adhesives*, vol. 118, Oct. 2022, doi: 10.1016/j.ijadhadh.2022.103232.
- [15] ATAY, Reyhan Deniz. "Failure Analysis in Adhesively Bonded Composite Joints." Master's Thesis, Middle East Technical University, 2019.
- [16] X. Ma et al., "Manufacture and Characterization of Carbon Fiber Composite Stiffened Skin by Resin Film Infusion/Prepreg Co-curing Process," *Journal of Reinforced Plastics and Composites*, vol. 33, no. 17, pp. 1559–1573, 2014, doi: 10.1177/0731684414543213.
- [17] C. Leone and S. Genna, "Effects of Surface Laser Treatment on Direct Co-bonding Strength of CFRP Laminates," *Composite Structures*, vol. 194, no. February, pp. 240–251, 2018, doi: 10.1016/j.compstruct.2018.03.096.
- [18] ASTM D5573\_99 Standard. Practice for Classifying Failure Modes in Fiber-Reinforced-Plastic (FRP) Joints. 1999.
- [19] Joannie W. Chin, "Surface Characterization and Adhesive Bonding of Carbon Fiber-Reinforced Composites," Doctoral dissertation, Virginia Polytechnic Institute and State University, 1994.
- [20] P. Molitor, V. Barron, and T. Young, "Surface Treatment of Titanium for Adhesive Bonding to Polymer Composites: A review," *International Journal of Adhesion and Adhesives*, vol. 21, no. 2, pp. 129–136, 2001, doi: 10.1016/S0143-7496(00)00044-0.
- [21] Y. M. Shin, M. M. Hohman, M. P. Brenner, and G. C. Rutledge, "Experimental Characterization of Electrospinning: The Electrically Forced Jet and Instabilities," *Polymer (Guildf)*, vol. 42, no. 25, pp. 09955–09967, 2001, doi: 10.1016/s0032-3861(01)00540-7.
- [22] Z. M. Huang, Y. Z. Zhang, M. Kotaki, and S. Ramakrishna, "A Review on Polymer Nanofibers by Electrospinning and Their Applications in Nanocomposites," *Composites Science and Technology*, vol. 63, no. 15, pp. 2223–2253, 2003, doi: 10.1016/S0266-3538(03)00178-7.
- [23] ÖZÇINAR, Zeynep Cansu, "Production of Nanofibers by Electrospinning for Interfacial Toughening Of Composites." Master's Thesis, Middle East Technical University, 2019.
- [24] K. Garg and G. L. Bowlin, "Electrospinning Jets and Nanofibrous Structures," *Biomicrofluidics*, vol. 5, no. 1, 2011, doi: 10.1063/1.3567097.

- [25] A. Mohan et al., "A Review on Polymer Nanofibers by electrospinning and Their Applications in Nanocomposites," *Composites Science and Technology*, vol. 63, no. 15, pp. 2223–2253, 2004, doi: 10.1016/S0266-3538(03)00178-7.
- [26] T. Subbiah, G. S. Bhat, R. W. Tock, S. Parameswaran, and S. S. Ramkumar, "Electrospinning of Nanofibers," *Journal of Applied Polymer Science*, vol. 96, no. 2, pp. 557–569, 2005, doi: 10.1002/app.21481.
- [27] Y. M. Shin, M. M. Hohman, M. P. Brenner, and G. C. Rutledge, "Electrospinning: A Whipping Fluid Jet Generates Submicron Polymer Fibers," *Applied Physics Letters*, vol. 78, no. 8, pp. 1149–1151, 2001, doi: 10.1063/1.1345798.
- [28] O. Hardick, B. Stevens, and D. G. Bracewell, "Nanofibre Fabrication in a Temperature and Humidity Controlled Environment for Improved Fibre Consistency," *Journal of Materials Science*, vol. 46, no. 11, pp. 3890–3898, Jun. 2011, doi: 10.1007/s10853-011-5310-5.
- [29] A. Haider, S. Haider, and I. K. Kang, "A Comprehensive Review Summarizing the Effect of Electrospinning Parameters and Potential Applications of Nanofibers in Biomedical and Biotechnology," *Arabian Journal of Chemistry*, vol. 11, no. 8. Elsevier B.V., pp. 1165–1188, Dec. 01, 2018. doi: 10.1016/j.arabjc.2015.11.015.
- [30] V. Jacobs, R. D. Anandjiwala, and M. Maaza, "The Influence of Electrospinning Parameters on the Structural Morphology and Diameter of Electrospun Nanofibers," *Journal of Applied Polymer Science*, vol. 115, no. 5, pp. 3130–3136, Mar. 2010, doi: 10.1002/app.31396.
- [31] Ş. Sirin, S. Çetiner, and As. Saraç, "Polymer Nanofibers Via Electrospinning: Factors Affecting Nanofiber Quality," *KSU. Journal of Engineering Sciences*, 2013.
- [32] S. Zargham, S. Bazgir, A. Tavakoli, A. S. Rashidi, and R. Damerchely, "The Effect of Flow Rate on Morphology and Deposition Area of Electrospun Nylon 6 Nanofiber." *Journal of Engineered Fibers and Fabrics*, vol. 7, no.4, 2012.
- [33] N. Bhardwaj and S. C. Kundu, "Electrospinning: A Fascinating Fiber Fabrication Technique," *Biotechnology Advances*, vol. 28, no. 3. pp. 325–347, May 2010. doi: 10.1016/j.biotechadv.2010.01.004.
- [34] J. H. Kweon, J. W. Jung, T. H. Kim, J. H. Choi, and D. H. Kim, "Failure of Carbon Composite-to-Aluminum Joints with Combined Mechanical Fastening and Adhesive Bonding," *Composite Structures*, vol. 75, no. 1–4, pp. 192–198, Sep. 2006, doi: 10.1016/j.compstruct.2006.04.013.
- [35] M. G. Song et al., "Effect of Manufacturing Methods on The Shear Strength of Composite Single-Lap Bonded Joints," *Composite Structures*, vol. 92, no. 9, pp. 2194–2202, 2010, doi: 10.1016/j.compstruct.2009.08.041.

- [36] R. H. Sanatgar, S. Borhani, S. A. H. Ravandi, and A. A. Gharehaghaji, "The Influence of Solvent Type and Polymer Concentration on the Physical Properties of Solid State Polymerized PA66 Nanofiber Yarn," *Journal of Applied Polymer Science*, vol. 126, no. 3, pp. 1112–1120, Nov. 2012, doi: 10.1002/app.36871.
- [37] B. Beylergil, M. Tanoğlu, and E. Aktaş, "Enhancement of Interlaminar Fracture Toughness of Carbon Fiber–Epoxy Composites Using Polyamide-6,6 Electrospun Nanofibers," *Journal of Applied Polymer Science*, vol. 134, no. 35, pp. 1–12, 2017, doi: 10.1002/app.45244.
- [38] T. Brugo and R. Palazzetti, "The Effect of Thickness of Nylon 6,6 Nanofibrous Mat on Modes I–II Fracture Mechanics of UD and Woven Composite Laminates," *Composite Structures*, vol. 154, pp. 172–178, 2016, doi: 10.1016/j.compstruct.2016.07.034.
- [39] L. Daelemans, S. van der Heijden, I. De Baere, H. Rahier, W. Van Paepegem, and K. De Clerck, "Nanofibre Bridging as a Toughening Mechanism in Carbon/Epoxy Composite Laminates Interleaved with Electrospun Polyamide Nanofibrous Veils," *Composites Science and Technology*, vol. 117, pp. 244–256, 2015, doi: 10.1016/j.compscitech.2015.06.021.
- [40] Ş. Parlayıcı, A. Avcı, and E. Pehlivan, "Electrospinning of Polymeric Nanofiber (Nylon 6,6/Graphene Oxide) for Removal of Cr (VI): Synthesis and Adsorption Studies," *Journal of Analytical Science and Technology*, vol. 10, no. 1, Dec. 2019, doi: 10.1186/s40543-019-0173-5.
- [41] E. Maccaferri, L. Mazzocchetti, T. Benelli, A. Zucchelli, and L. Giorgini, "Morphology, Thermal, Mechanical Properties and Ageing of Nylon 66/Graphene Nanofibers as Nano<sup>2</sup> Materials," *Composites Part B: Engineering*, vol. 166, pp. 120–129, Jun. 2019, doi: 10.1016/j.compositesb.2018.11.096.
- [42] J. Kim, J. Oh, K. Y. Lee, I. Jung, and M. Park, "Dispersion of Graphene-Based Nanocarbon Fillers in Polyamide 66 by Dry Processing and Its Effect on Mechanical Properties," *Composites Part B: Engineering*, vol. 114, pp. 445–456, Apr. 2017, doi: 10.1016/j.compositesb.2017.01.054.
- [43] E. Cakal Sarac, L. Haghghi Poudeh, I. Berktas, and B. Saner Okan, "Scalable Fabrication of High-Performance Graphene/Polyamide 66 Nanocomposites with Controllable Surface Chemistry by Melt Compounding," *Journal of Applied Polymer Science*, vol. 138, no. 10, Mar. 2021, doi: 10.1002/app.49972.
- [44] J. Mohan, A. Ivanković, and N. Murphy, "Mixed-Mode Fracture Toughness of Co-cured and Secondary Bonded Composite Joints," *Engineering Fracture Mechanics*, vol. 134, pp. 148–167, 2015, doi: 10.1016/j.engfracmech.2014.12.005.
- [45] S. van der Heijden et al., "Interlaminar Toughening of Resin Transfer Moulded Glass Fibre Epoxy Laminates by Polycaprolactone Electrospun Nanofibres," *Composites Science and Technology*, vol. 104, pp. 66–73, 2014, doi: 10.1016/j.compscitech.2014.09.005.

- [46] D. Saz-orozco, D. Ray, and W. F. Stanley, "Effect of Thermoplastic Veils on Interlaminar Fracture Toughness of a Glass Fiber / Vinyl Ester Composite," *Polymer Composites*, 2015, doi: 10.1002/pc.
- [47] G. W. Beckermann and K. L. Pickering, "Mode I and Mode II Interlaminar Fracture Toughness of Composite Laminates Interleaved with Electrospun Nanofibre Veils," *Composites Part A: Applied Science and Manufacturing*, vol. 72, pp. 11–21, 2015, doi: 10.1016/j.compositesa.2015.01.028.
- [48] G. Esenoğlu et al., "Improving Adhesive Behavior of Fiber Reinforced Composites by Incorporating Electrospun Polyamide-6,6 Nanofibers in Joining Region," *Journal of Composite Materials*, vol. 56, no. 29, pp. 4449–4459, Dec. 2022, doi: 10.1177/00219983221133478.
- [49] "Prepreg." HEXCEL. Accessed July 12, 2023.  
<https://www.hexcel.com/Resources/DataSheets/Prepreg>.
- [50] "FM 300." Solvay. Accessed July 12, 2023.  
<https://www.solvay.com/en/product/fm-300>.
- [51] "Naylon 6/6." Sigma Aldrich. Accessed July 12, 2023.  
<https://www.sigmaaldrich.com/TR/en/product/aldrich/42917>.
- [52] "RGO." Nanografi. Accessed July 12, 2023.  
<https://shop.nanografi.com.tr/ndirgenmi-grafen-oksit-rgo-2-5-katman-y-a-1562-m2-g/>.